The architecture of the diaminobutyrate acetyltransferase active site provides mechanistic insight into the biosynthesis of the chemical chaperone ectoine

Received for publication, September 30, 2019, and in revised form, January 19, 2020 Published, Papers in Press, January 22, 2020, DOI 10.1074/jbc.RA119.011277

Alexandra A. Richter[‡§], Stefanie Kobus[¶], Laura Czech[‡§1], Astrid Hoeppner[¶], Jan Zarzycki[‖], Tobias J. Erb[§‖], Lukas Lauterbach[**], Jeroen S. Dickschat[**], Erhard Bremer[‡§2], and Sander H. J. Smits[¶‡‡3]

From the [‡]Department of Biology, Laboratory for Microbiology, and the [§]SYNMIKRO Research Center, Philipps-University Marburg, D-35043 Marburg, Germany, the [¶]Center for Structural Studies and the [‡‡]Institute of Biochemistry, Heinrich-Heine University Düsseldorf, Düsseldorf, Germany, the [‖]Department of Biochemistry and Synthetic Metabolism, Max-Planck-Institute for Terrestrial Microbiology, D-35043 Marburg, Germany, and the [**]Kekulé-Institute for Organic Chemistry and Biochemistry, Friedrich-Wilhelms-University Bonn, D-53121 Bonn, Germany

Edited by Wolfgang Peti

Ectoine is a solute compatible with the physiologies of both prokaryotic and eukaryotic cells and is widely synthesized by bacteria as an osmotic stress protectant. Because it preserves functional attributes of proteins and macromolecular complexes, it is considered a chemical chaperone and has found numerous practical applications. However, the mechanism of its biosynthesis is incompletely understood. The second step in ectoine biosynthesis is catalyzed by L-2,4-diaminobutyrate acetyltransferase (EctA; EC 2.3.1.178), which transfers the acetyl group from acetyl-CoA to EctB-formed L-2,4-diaminobutyrate (DAB), yielding *N*-γ-acetyl-L-2,4-diaminobutyrate (*N*-γ-ADABA), the substrate of ectoine synthase (EctC). Here, we report the biochemical and structural characterization of the EctA enzyme from the thermotolerant bacterium *Paenibacillus lautus* (*Pl*). We found that (*Pl*)EctA forms a homodimer whose enzyme activity is highly regiospecific by producing *N*-γ-ADABA but not the ectoine catabolic intermediate *N*-α-acetyl-L-2,4-diaminobutyric acid. High-resolution crystal structures of (*Pl*)EctA (at 1.2–2.2 Å resolution) (i) for its apo-form, (ii) in complex with CoA, (iii) in complex with DAB, (iv) in complex with both CoA and DAB, and (v) in the presence of the product *N*-γ-ADABA were obtained. To pinpoint residues involved in DAB binding, we probed the structure-function relationship of (*Pl*)EctA by site-directed mutagenesis. Phylogenomics shows that EctA-type proteins from both Bacteria and Archaea are evolutionarily highly conserved, including catalytically important residues. Collectively, our biochemical and structural findings yielded detailed insights into the catalytic core of the EctA enzyme that laid the foundation for unraveling its reaction mechanism.

Compatible solutes are a distinct group of highly water-soluble organic osmolytes that are compliant with the biochemistry and physiology of both prokaryotic and eukaryotic cells (1–3). The function-preserving attributes of these solutes for proteins and other cellular components (4–9) led to their description as chemical chaperones (10–12). Building on the special physico-chemical characteristics of these compounds, many members of the Bacteria, Archaea, and Eukarya use compatible solutes as cytoprotectants against different types of environmental and cellular challenges (1–3, 13–15).

Compatible solutes have been widely adopted by microorganisms as osmotic stress protectants (3, 16–18). Their amassing, either through synthesis or uptake (13), increases the osmotic potential of the cytoplasm and prevents a long-lasting increase in the ionic strength of this cell compartment (19, 20) under osmotically unfavorable conditions. As an immediate result of compatible solute accumulation, high osmolarity–triggered water efflux from the cell is counteracted. This in turn prevents drop of vital turgor to physiologically nonsustainable values and averts an undue increase in molecular crowding of the cytoplasm (19–22).

Ectoine ((*S*)-2-methyl-1,4,5,6-tetrahydropyrimidine-4-carboxylic acid) (23) and its derivative 5-hydroxyectoine ((4*S*,5*S*)-5-hydroxy-2-methyl-1,4,5,6-tetrahydropyrimidine-4-carboxylic acid) (24) are prominent members of the type of compatible solutes used by microorganisms (3). They are widely synthesized by bacteria (25, 26), by a restricted number of archaea (27), and notably, also by a few halophilic protists (28–30) and some microalgae (31). Synthesis of ectoine starts from L-aspar-

This work was supported in part by grants from the Deutsche Forschungsgemeinschaft (DFG) through SFB 987 (Philipps-University Marburg) (to E. B. and T. J. E.) and the DFG-funded Transregio SFB TR41 (Braunschweig/Oldenburg/Bonn/Göttingen) (to J. S. D.). The Center for Structural studies is supported by the DFG as well (Grant 417919780, INST 208/740-1 FUGG). The authors declare that they have no conflicts of interest with the contents of this article.

This article contains Tables S1 and S2, Figs. S1–S5, and Video S1.

The atomic coordinates and structure factors (codes 6SLK, 6SK1, 6SL8, 6SJY, and 6SLL) have been deposited in the Protein Data Bank (http://wwpdb.org/). The nucleotide sequence(s) reported in this paper has been submitted to the GenBank™/EBI Data Bank with accession number(s)MF327591.1.

[1] Supported by a Ph.D. fellowship from the International Max Planck Research School for Environmental, Cellular and Molecular Microbiology (IMPRS-Mic, Marburg).

[2] To whom correspondence may be addressed: Dept. of Biology, Laboratory for Microbiology, Philipps-University Marburg, Karl-von-Frisch Str. 8, D-35043 Marburg, Germany. Tel.: 49-6421-2821529; Fax: 49-6421-2828979; E-mail: bremer@staff.uni-marburg.de.

[3] To whom correspondence may be addressed: Institute of Biochemistry, Heinrich-Heine-University Düsseldorf, Universitätsstrasse 1, D-40225 Düsseldorf, Germany. Tel.: 49-2118-112647; Fax: 49-211-8115310; E-mail: sander.smits@hhu.de.

tate-β-semialdehyde, a central hub in bacterial amino acid and cell wall synthesis (32–36). Ectoine is formed by sequential reactions of L-2,4-diaminobutyrate transaminase (EctB;[4] EC 2.6.1.76), L-2,4-diaminobutyrate acetyltransferase (EctA; EC 2.3.1.178), and ectoine synthase (EctC; EC 4.2.1.108) (34, 36). A substantial subgroup of ectoine producers can modify ectoine to yield 5-hydroxyectoine, a biotransformation catalyzed by the ectoine hydroxylase (EctD; EC 1.14.11.55) (37–39). Compared with ectoine, 5-hydroxyectoine often possesses enhanced, or additional, protective attributes against various types of cellular and environmental constraints (26, 40, 41). Reflecting the osmostress-protective role of ectoines in microbial physiology, their enhanced production is typically triggered when microbial cells are exposed to high osmolarity surroundings. This process is largely caused by a strong up-regulation in the transcription of the *ectABC(D)* biosynthetic genes (26, 40–44).

Ectoines can also protect microorganisms against the detrimental effects of extremes in either high or low growth temperatures (39, 45–47). They can preserve the functionality of proteins against various types of challenges (8, 9, 48–51), ameliorate desiccation stress (52, 53), influence membrane fluidity and stabilize lipid bilayers (54, 55), protect DNA from damage by ionizing radiation (56, 57), enhance structural changes in DNA (58, 59), provide oxidative stress resistance (60), and possess hydroxyl radical scavenging activities (61). Building on the function-preserving and anti-inflammatory properties of ectoines, various types of medical applications of ectoines are also increasingly pursued (62–65).

Reflecting their function as chemical chaperones, ectoines have already found a considerable number of commercial applications (26, 40, 66). To satisfy the increased demand for ectoines, an industrial scale biotechnological production process has been developed that uses the highly salt-tolerant bacterium *Halomonas elongata* as a natural and engineered cell factory (67); it is able to deliver ectoines on the scale of tons annually (40). Hence, both from the perspective of basic science and the biotechnological production of ectoines, a deeper understanding of the properties of the ectoine/5-hydroxyectoine biosynthetic enzymes is desirable (34, 36, 68). Substantial advances in this context have recently been made though detailed biochemical and structural studies of EctB (69), EctC (25, 70), and EctD (71–73). In contrast, EctA, the focus of this study, is far less well-understood.

EctA catalyzes the second step in ectoine biosynthesis (34, 36, 41) and belongs to the superfamily of GCN5-related *N*-acetyltransferases (GNAT) (74, 75). These types of enzymes catalyze the transfer of an acetyl group from acetyl-CoA to an amino group of a range of acceptor molecules (74, 75). In the case of EctA, L-2,4-diaminobutyrate (DAB), the reaction product of the EctB enzyme (69), is acetylated to yield *N*-γ-acetyl-L-2,4-diaminobutyrate (*N*-γ-ADABA) (34, 68) (Fig. 1*A*). This intermediate is the substrate of the ectoine synthase EctC, which forms the cyclic ectoine molecule through a water elimination reaction (25, 34, 36).

Basic biochemical properties of EctA enzymes from *H. elongata* and several methylotrophs have been reported (34, 35, 68, 76). However, a thorough understanding of EctA is still lacking, and in particular, crystal structures in complex with its substrates and/or its reaction product are missing. To fill this gap, we report here biochemical and structural characteristics of EctA from the thermotolerant bacterium *Paenibacillus lautus* (*Pl*) (77) in its apo, substrate, and co-substrate–bound forms and a crystal structure trapping the reaction product. Collectively, this crystallographic analysis, combined with site-directed mutagenesis experiments, illuminates the architecture of the active site of the EctA L-2,4-diaminobutyrate acetyltransferase and allows a proposal for its enzyme reaction mechanism.

Results and discussion

Overproduction and purification of (Pl)EctA

Ectoine/5-hydroxyectoine-producing microorganisms can populate ecological niches with rather different biological and physico-chemical characteristics (26, 40, 41). One of these ectoine-producing microorganisms is the *P. lautus* strain Y4.12MC10, a Gram-positive spore-forming intestinal bacterium that was originally isolated from the effluent of the Obsidian hot spring in Yellowstone National Park (77). We explored the suitability of the (*Pl*)EctA protein for biochemical and crystallographic analysis.

For the heterologous production of (*Pl*)EctA in *Escherichia coli*, we constructed expression vectors using a codon-optimized version of the (*Pl*)*ectA* gene (GenBank™ accession number MF327591.1). These constructs yielded (*Pl*)EctA proteins with either a N-terminal (NH_2-WSHPQFEK-SG) or a C-terminal (SA-WSHPQFEK-COOH) *Strep*-Tag II peptide for their purification by affinity chromatography. The corresponding synthetic (*Pl*)*ectA* constructs were expressed under the control of the plasmid-based TetR-regulated *tet* promoter. Both the *Strep*-Tag II-(*Pl*)EctA and the (*Pl*)EctA-*Strep*-Tag II proteins could be purified to apparent homogeneity (Fig. 1*B*). Both versions of the (*Pl*)EctA protein show a dimeric state in solution, as assessed by size-exclusion chromatography coupled to multiangle light scattering (SEC-MALS) (78). This is documented for the (*Pl*)EctA-*Strep*-Tag II protein in Fig. 1*C* and revealed a molecular mass of 39.73 ± 0.04 kDa. The calculated theoretical molecular masses of the recombinant monomers are 20.68 kDa (*Strep*-Tag II-(*Pl*)EctA) and 20.25 kDa ((*Pl*)EctA-*Strep*-Tag II), respectively. Thus, the SEC-MALS data suggest that the (*Pl*)EctA protein is a stable dimer in solution, in line with previous reports that the EctA proteins from *H. elongata* and from the methylotrophs *Methylomicrobium alcaliphilum*, *Methylophaga alcalica*, and *Methylophaga thalassica* are also dimers in solution (34, 68). Collectively, these findings suggest

[4] The abbreviations used are: EctB, L-2,4-diaminobutyrate transaminase; EctA, L-2,4-diaminobutyrate acetyltransferase; EctC, ectoine synthase; EctD, DAB, L-2,4-diaminobutyrate; *N*-γ-ADABA, *N*-γ-acetyl-L-2,4-diaminobutyrate; *N*-α-ADABA, *N*-α-acetyl-L-2,4-diaminobutyrate; ASU, asymmetric unit; AHT, anhydrotetracycline; FMOC, fluorenylmethyloxycarbonyl; DTNB, dithionitrobenzoic acid; GNAT, GCN5-related *N*-acetyltransferase(s); DAB, L-2,4-diaminobutyrate; SEC, size-exclusion chromatography; MALS, multiangle light scattering; PDB, Protein Data Bank; r.m.s.d., root mean square deviation; OD, optical density; CHES, 2-(cyclohexylamino)ethanesulfonic acid; TES, 2-{[2-hydroxy-1,1-bis(hydroxymethyl)ethyl]amino}ethanesulfonic acid; Bistris propane, 1,3-bis[tris(hydroxymethyl)methylamino]propane.

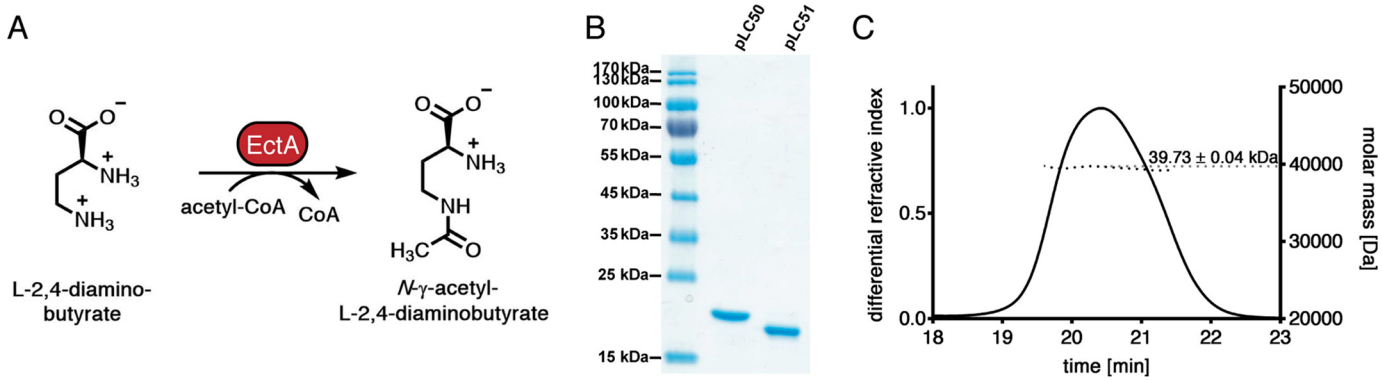

Figure 1. (*Pl*)EctA-catalyzed enzyme reaction, purification, and quaternary assembly of the (*Pl*)EctA protein. *A*, (*Pl*)EctA enzyme catalyzes the transfer of the acetyl-moiety from acetyl-CoA onto the substrate L-2,4-diaminobutyrate, resulting in the formation of *N*-γ-acetyl-L-2,4-diaminobutyrate and free CoA as reaction products. *B*, Coomassie-stained SDS-PAGE of purified *Strep*-tag II-(*Pl*)EctA (pLC50) protein and (*Pl*)EctA-*Strep*-tag II protein (pLC51) (2 μg of each protein were loaded onto the SDS gel). The size standard is given in kDa. *C*, MALS-RI analysis shows that the (*Pl*)EctA protein elutes with an absolute molecular mass of 39.73 ± 0.04 kDa, consistent with the notion that it is a homodimer in solution. The calculated theoretical molecular mass of the monomer of the *Strep*-tag II-(*Pl*)EctA and of the (*Pl*)EctA-*Strep*-tag II recombinant proteins is 20.68 and 20.25 kDa, respectively.

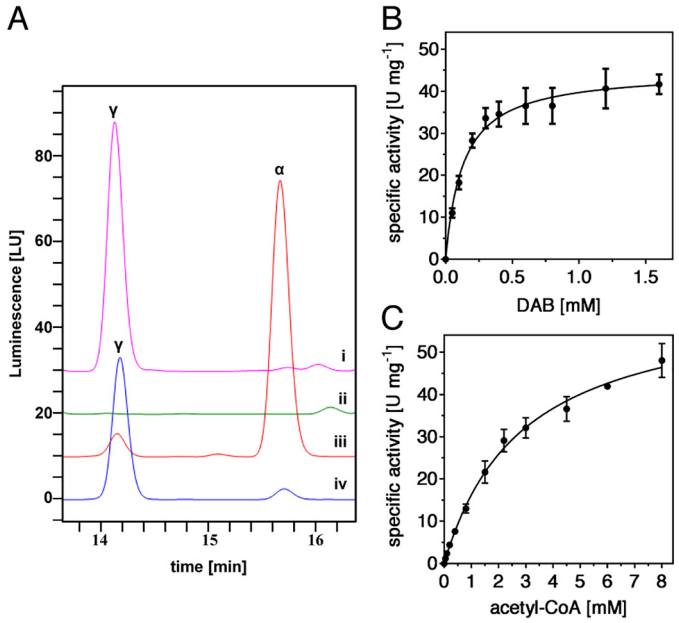

Figure 2. (*Pl*)EctA-dependent *N*-γ-acetyl-L-2,4-diaminobutyrate production and kinetic parameters of the (*Pl*)EctA enzyme. *A*, HPLC traces showing the regio-selective acetylation of DAB by (*Pl*)EctA with only *N*-γ-ADABA, and not its isomer *N*-α-ADABA, as product (*i*). (*ii*) in the negative control sample (reaction mix, without enzyme) no ADABA can be detected. As references, chemical synthesized *N*-α-ADABA (*iii*) and *N*-γ-ADABA (*iv*) were used. The velocity of (*Pl*)EctA at increasing concentrations of the substrates DAB (*B*) and acetyl-CoA (*C*) was determined. *Error bars*, S.D. calculated from two biological and two technical replicas each. *LU*, luminescence units.

that dimer formation is probably a general feature of EctA-type L-2,4-diaminobutyrate acetyltransferases.

Analysis of the purified *Strep*-Tag II-(*Pl*)EctA and (*Pl*)EctA-*Strep*-Tag II proteins by SDS-PAGE revealed a significant difference in their migration behavior (Fig. 1*B*) that was not expected from their almost identical calculated theoretical molecular masses. We therefore performed an electrospray ionization-MS analysis of both recombinant proteins. The molecular masses determined by this technique revealed values of 20.55 kDa for the *Strep*-Tag II-(*Pl*)EctA protein and 20.12 kDa for the (*Pl*)EctA-*Strep*-Tag II protein, respectively. Hence, in both cases, the experimentally determined masses correlate with the calculated theoretical masses of the recombinant proteins minus 0.13 kDa. This finding could possibly indicate a posttranslational elimination of the N-terminal methionine residues during heterologous production and purification of the two N-terminal and C-terminal *Strep*-Tag II–marked (*Pl*)EctA proteins. The reason for the notable difference in their migration behavior on 15% SDS-polyacrylamide gels is not apparent.

Kinetic parameters of (Pl)EctA

In the ectoine biosynthesis route, *N*-γ-ADABA is the expected product of the EctA-catalyzed enzyme reaction (34, 36, 41). In contrast, its isomer *N*-α-acetyl-L-2,4-diaminobutyric acid (*N*-α-ADABA) is formed as an intermediate during the catabolism of ectoine when microorganisms use this nitrogen-rich compound as a nutrient (67, 79). Notably, *N*-α-ADABA, but not *N*-γ-ADABA, serves as the inducer for the MocR/GabR-type EnuR regulatory protein (80) controlling the expression of many ectoine catabolic gene clusters (41, 81). To ascertain that the (*Pl*)EctA enzyme exclusively synthesizes *N*-γ-ADABA from L-2,4-diaminobutyrate and acetyl-CoA (34, 36) (Fig. 1*A*), we performed an enzyme assay in which we subsequently benchmarked the formed reaction product(s) against chemically synthesized and purified *N*-γ-ADABA and *N*-α-ADABA reference samples. We used for this experiment an HPLC analysis protocol allowing the separation of the two ADABA isomers (70, 82). Our analysis showed that the (*Pl*)EctA enzyme indeed exclusively synthesizes *N*-γ-ADABA under *in vitro* assay conditions (Fig. 2*A*). Therefore, we conclude that the EctA L-2,4-diaminobutyrate acetyltransferase transfers the acetyl group from the co-substrate to the substrate in a highly position-specific manner.

For the initial enzyme assays, we determined basic biochemical characteristics of the recombinant (*Pl*)EctA-*Strep*-Tag II protein, including its pH optimum, its salt tolerance, and its optimal temperature. The (*Pl*)EctA enzyme showed a broad pH optimum under alkaline conditions (pH 8.5–9.5), maintaining 75% of its activity at pH 10 (Fig. S1*A*). The enzyme was sensitive against extreme acidic conditions, as less then 10% of enzyme activity was retained at pH 6.0. Based upon these data, we performed all subsequent enzyme assays at pH 7.5 (75% EctA activ-

Table 1
Data collection and refinement statistics for the apo form of EctA and the substrate-bound forms
Values in parentheses are for the outer shell.

	Apo-EctA	CoA-EctA	DAB-CoA-EctA	DAB-EctA	*N*-γ-ADABA
Crystal parameters					
X-ray source	ID30B, ESRF, Grenoble	ID29, ESRF, Grenoble	ID29, ESRF, Grenoble	ID30A-3, ESRF, Grenoble	ID23–1, ESRF, Grenoble
Detector	Pilatus3_6M	Pilatus_6M_F	Pilatus_6M_F	EIGER_4M	Pilatus_6M_F
Space group	P 41 21 2	P 43 21 2	R 3	P 43 21 2	P 41 21 2
Unit cell parameters					
a, *b*, *c* (Å)	176.01, 176.01, 61.78	68.27, 68.27, 79.79	151.21, 151.21, 46.22	57.98, 57.98, 134.46	174.22, 174.22, 60.99
α, β, γ (degrees)	90, 90, 90	90, 90, 90	90, 90, 120	90, 90, 90	90, 90, 90
Data collection and processing					
Resolution (Å)	124.5–1.95 (2.07–1.95)	51.89–1.13 (1.21–1.13)	75.53–1.05 (1.11–1.05)	53.24–1.51 (1.60–1.51)	123.2–2.02 (2.15–2.02)
Unique reflections	70,540 (10,980)	70,942 (12,931)	182,408 (27,168)	36,817 (5,756)	61,414 (9,533)
Completness (%)	99.2 (95.5)	99.9 (99.8)	99.2 (96.3)	99.9 (99.9)	99.5 (97.2)
Redundancy	12.9 (13.1)	8.3 (7.8)	3.59 (3.19)	8.8 (8.8)	13.1 (12.4)
I/σ	10.65 (1.08)	13.46 (1.23)	10.43 (1.59)	16.64 (1.32)	17.44 (2.45)
R_{sym}	0.161 (2.588)	0.067 (1.343)	0.048 (0.608)	0.058 (1.453)	0.092 (1.105)
Refinement statistics					
Resolution (Å)	124.5–2.20	51.883–1.50	75.53–1.20	53.40–1.53	123.2–2.20
R_{work} (%)	0.1695 (0.2370)	0.1468 (0.143)	0.1218 (0.2560)	0.1775 (0.3100)	0.1674 (0.2250)
R_{free} (%)	0.2050 (0.2690)	0.1834 (0.185)	0.1496 (0.2680)	0.2140 (0.3220)	0.2070 (0.2700)
r.m.s.d. from ideal					
Bond lengths (Å)	0.020	0.028	0.039	0.024	0.021
Bond angles (degrees)	1.983	2.597	3.024	2.345	2.145
Average *B*-factors (Å^2)	43.0	15.0	18.0	32.00	44.0
Ramachandran plot					
Most favored (%)	97.4	99.3	97.9	97.4	97.8
Allowed (%)	2.6	0.7	2.1	2.6	2.0
Disallowed (%)	0.0	0.0	0.0	0.0	0.2
Model content					
Monomers/ASU	3	1	2	1	3
Protein residues	7–168, 2–176, 7–168	8–167	6–169, 6–171	8–168	4–170, 2–176, 7–168
Ligands		CoA	CoA, DAB	DAB	ADABA
Water molecules	281	209	543	146	220
PDB code	6SLK	6SK1	6SLL	6SL8	6SJY

ity) to prevent spontaneous hydrolysis of acetyl-CoA under alkaline conditions.

The tolerance of the (*Pl*)EctA enzyme against increased concentrations of NaCl was rather modest: a content of 100 mM NaCl in the assay solution already led to a notable decrease of the enzyme activity (down to 75%), and only about 12% of the enzyme activity remained when the NaCl content of the reaction buffer was increased to 1.5 M (Fig. S1*B*). The salt sensitivity of the (*Pl*)EctA enzyme contrasts sharply with the enzymatic characteristics of the EctB L-2,4-diaminobutyrate transaminase (69) and of the EctC ectoine synthase (25) from *P. lautus* Y4.12MC10, as these are highly salt-tolerant enzymes. Differences with respect to the behavior of EctA-type enzymes from various microorganisms toward NaCl have already been reported. Moderate concentrations of NaCl (0.2–0.4 M) activate the corresponding enzymes from *H. elongata* and *M. alcaliphilum*. However, increased NaCl concentrations inhibit those of *M. thalassica* and *M. alcalica* (34, 68), a feature shared by the *P. lautus* EctA enzyme (Fig. S1*B*).

Keeping the thermo-tolerant nature of the *P. lautus* Y4.12MC10 donor strain in mind (77), a substantial degree of thermo-resistance of the (*Pl*)EctA enzyme activity was expected. Predictably, the activity of the (*Pl*)EctA enzyme increased with increasing temperature (Fig. 1*C*). However, the purified protein was not very thermostable, as the enzyme was only active for very short times at temperatures higher than 40 °C. For instance, at 50 °C, the (*Pl*)EctA enzyme was highly active but only for a few seconds, whereupon the activity dropped precipitously.

Considering the results of these basic enzyme assays, and taking the spontaneous hydrolysis of acetyl-CoA under alkaline conditions and the instability of the (*Pl*)EctA protein at high temperatures into account, we devised an enzyme assay for the (*Pl*)EctA protein. It employed the following conditions: 100 mM TES buffer (pH 7.5), 4 mM acetyl-CoA or 5 mM DAB, respectively, and a temperature of 30 °C. The following apparent kinetic parameters for the (*Pl*)EctA were determined: (i) a K_m of 0.13 ± 0.03 mM and a V_{max} of 44.87 ± 2.66 units mg^{-1} for the substrate DAB and (ii) K_m of 2.79 ± 0.73 mM and a V_{max} of 58.27 ± 6.56 units mg^{-1} for acetyl-CoA (Fig. 2, *B* and *C*).

Crystal structure of apo-form of EctA reveals a homodimer

To gain insights into the molecular mechanisms of the EctA enzyme, we determined crystal structures of the apo-form of (*Pl*)EctA in the presence of the two substrates or its reaction product (Fig. 1*A*). First, we determined the crystal structure of the apo-(*Pl*)EctA protein; the obtained structure had a resolution of 2.2 Å (Table 1). The (*Pl*)EctA protein adopts the classical GNAT fold (74, 75) with a mixed parallel/antiparallel twisted β-sheet in its center, flanked by four α-helices. A short 3_{10}-helix (α5) is present on the extended outward-facing loop connecting β-strand 6 and β7 (Fig. 3, *A* and *B*).

To identify the structurally closest homologs of the (*Pl*)EctA protein, we performed a DALI search (83), which revealed a variety of acetyltransferases among the top hits. The structurally closest relative of (*Pl*)EctA is the EctA from the pathogen *Bordetella parapertussis* (*Bp*) in complex with the substrate DAB (PDB code 3D3S: r.m.s.d. of 1.3 Å over 158 Cα atoms). No

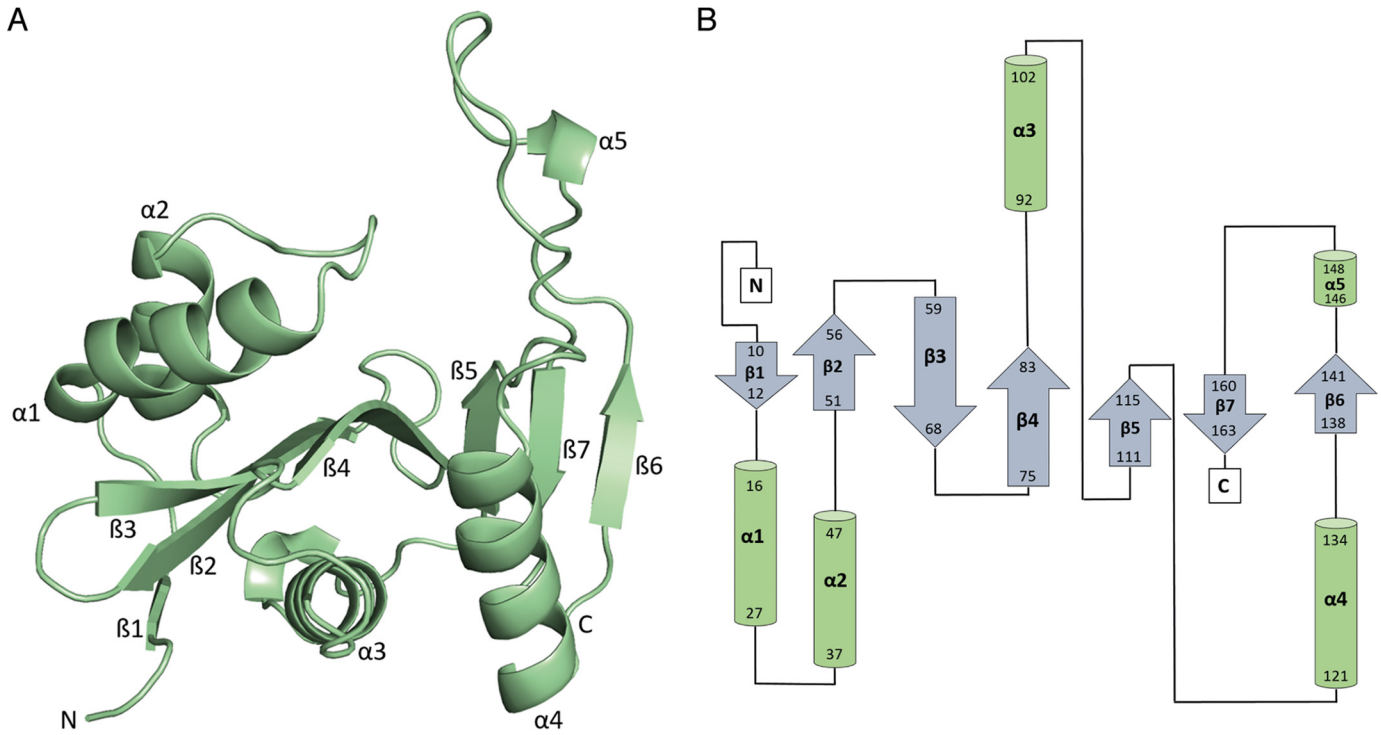

Figure 3. Overall fold of the (*Pl*)EctA monomeric subunit. *A*, cartoon representation of the (*Pl*)EctA monomeric subunit including the nomenclature of the secondary structure elements and the tertiary structure. *B*, schematic illustration of the secondary structure of (*Pl*)EctA.

detailed description of this crystal structure or publication describing the salient features of the (*Bp*)EctA enzyme is currently available. We discuss the position of the DAB ligand in the 3D3S crystal structure below, as it differs substantially from that which we found in the (*Pl*)EctA crystal structure.

Further inspection of the crystal packing, in line with our SEC-MALS analysis (Fig. 1*C*), revealed the presence of an (*Pl*)EctA homodimer within the asymmetric unit (AS). Two (*Pl*)EctA monomers are packed against each other mainly through helices α1 and α2, the short 3_{10}-helix α5, and strand β5 and their corresponding loop regions. Both monomers are rotated against each other by about 180° (Fig. 4, *A* and *B*). The interface area, as calculated with the PDBePISA online server (http://www.ebi.ac.uk/pdbe/prot_int/pistart.html),[5] is 1505.3 Å^2 and comprises 27 hydrogen bonds or salt bridges (Table S1). Notably, the dimeric assembly of (*Pl*)EctA also revealed that the side chain of Tyr^{38} from one monomer penetrates into the other and vice versa (Fig. 4*B*). This residue is part of the amino acid sequence ^{36}SPYCYMLLGD^{45} that forms helix α2 (Fig. 3*A*). The aromatic side chain of Tyr^{38} points toward the binding site of the DAB substrate (Fig. 4*B*) (see below).

The crystal structures of (Pl)EctA in complex with the co-substrate reveals an evolutionarily conserved CoA-binding site

Next, we determined the (*Pl*)EctA:CoA structure by molecular replacement using the apo-(*Pl*)EctA structure as a search model. This crystal structure has a resolution of 1.5 Å (Table 1). The CoA molecule could be unambiguously placed in the crystal structure and refined into a well-defined density present in the active site of (*Pl*)EctA (Fig. 5). A comparison of the apo- and CoA-bound structures of (*Pl*)EctA revealed no major overall differences, as indicated by an r.m.s.d. of only 0.4 Å over 150 Cα atoms.

In the (*Pl*)EctA:CoA complex, the CoA molecule (Fig. 5, *A* and *B*) is bound in a deep cleft formed by the loops connecting α1-α2, β4-α3, β5-α4, and helices α3 and α4 (Fig. 3), creating a mainly positively charged surrounding for the co-substrate (Fig. 5, *A* and *C*). The 3′-phosphate group of the adenosine moiety interacts with the side chains of Lys^{94} (at a distance of 2.9 Å) and Arg^{125} (at a distance of 3.0 Å), whereas the side chain of Arg^{89} acts as a clamp that, together with the helix α4, sandwiches the adenine moiety. As characteristic for GNAT superfamily enzymes, the "P-loop" is the signature motif for the CoA-pyrophosphate–binding site (74, 75, 84) and possesses the following consensus sequence: Gln/Arg-*X*-*X*-Gly-*X*-Gly/Ala. The amino acid sequence of this region present in the (*Pl*)EctA protein corresponds to residues Arg^{88}-Arg^{89}-Gln^{90}-Gly^{91}-Ile^{92}-Ala^{93}. The oxygen atoms of the pyrophosphate are involved in hydrogen bonding with the backbone nitrogen atoms of Arg^{89} (at a distance of 2.8 Å), Gln^{90} (at a distance of 3.3 Å), Gly^{91} (at a distance of 2.9 Å), Ala^{93} (at a distance of 2.9 Å), and Lys^{94} (at a distance of 2.9 Å). The pantothenate unit is hydrogen-bonded by its amide O atom to the backbone of Val^{83} (at a distance of 2.8 Å). The β-alanine carbonyl oxygen interacts with the side chain of Asn^{120} (2.8 Å) and the cysteamine nitrogen with the backbone hydroxyl group of Val^{81} (at a distance of 2.7 Å) (Fig. 5*C*). Although the overall fold of (*Pl*)EctA does not significantly differ upon substrate and/or cofactor binding, it is worth mentioning that the N-terminal part of the loop connecting helices α1 and α2 (*i.e.* amino acids 29–32) folds slightly

[5] Please note that the JBC is not responsible for the long-term archiving and maintenance of this site or any other third party hosted site.

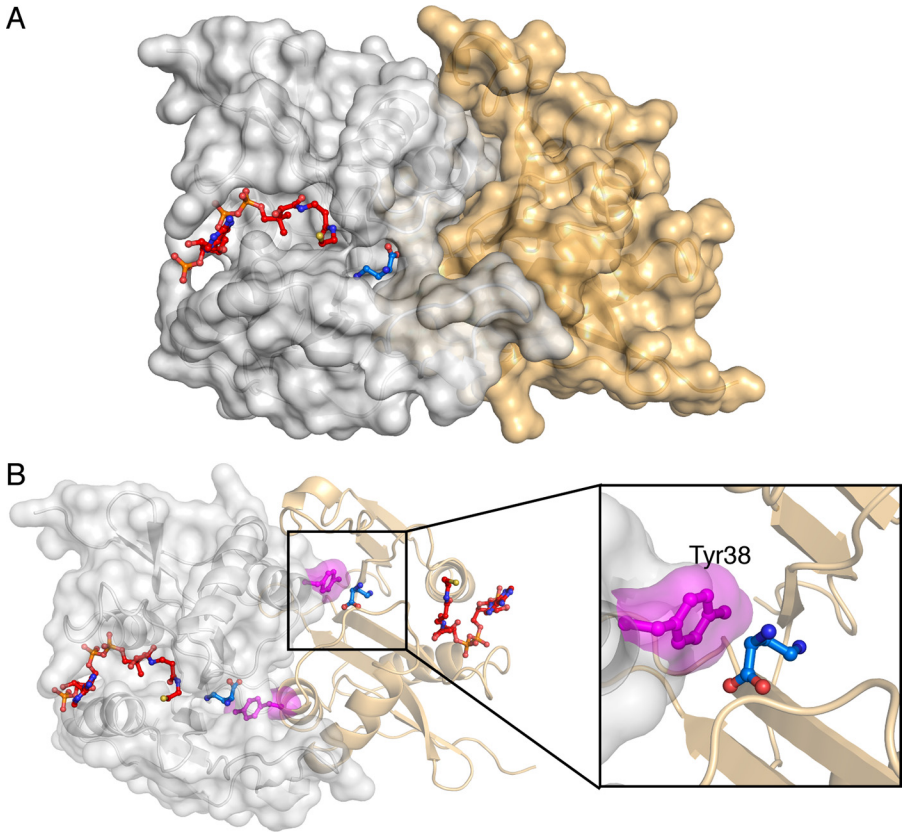

Figure 4. Dimer assembly of the (*Pl*)EctA enzyme. *A*, surface presentation of the dimer assembly of the (*Pl*)EctA protein displaying the binding site for the ligands CoA (*red*) and DAB (*blue*). *B*, illustration of the dimeric interface, highlighting the protrusion of the side chain of Tyr^{38} from monomer B into the DAB-binding site of monomer A (and vice versa). This graphical representation of the dimer assembly was rendered by using the (*Pl*)EctA:CoA:DAB tertiary crystal structure (PDB code 6SLL) as the template.

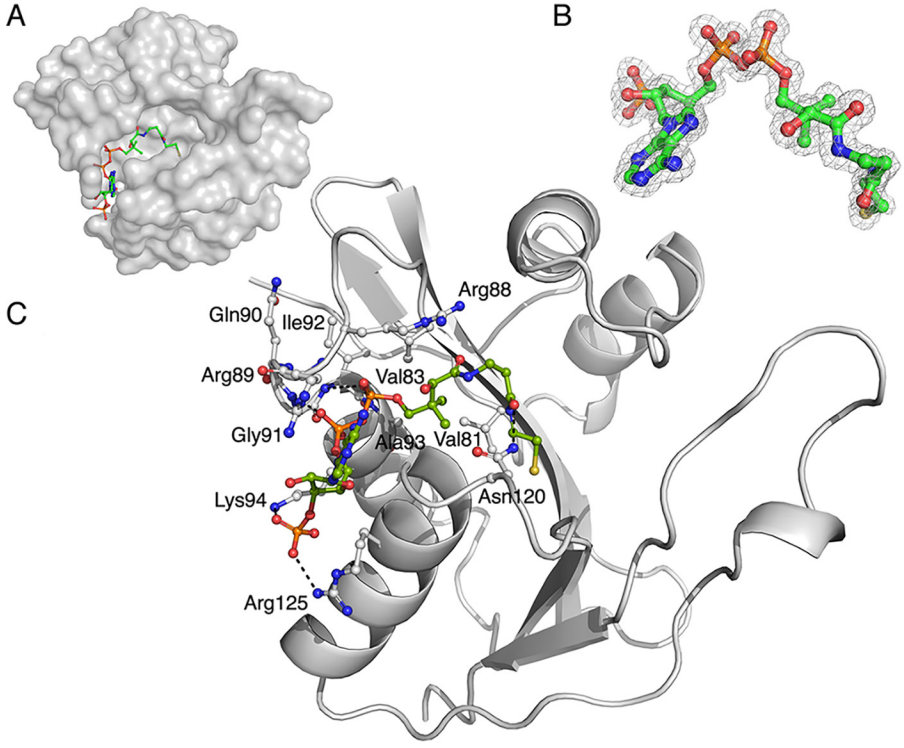

Figure 5. Architecture of the CoA-binding site. *A*, *surface presentation* of the monomeric subunit of the (*Pl*)EctA protein, illustrating the binding tunnel for CoA. *B*, electron density of the bound CoA ligand (contoured at 1σ). *C*, substrate-binding site for CoA, showing the amino acids involved in coordinating the CoA molecule within the (*Pl*)EctA active site.

closer toward α2 in the (*Pl*)EctA:CoA crystal structure, thereby enabling the tail of the cofactor to orient toward the substrate-binding site.

CoA-binding sites are evolutionarily highly conserved (75, 84). We therefore assessed whether this was also true for the corresponding binding site in the (*Pl*)EctA:CoA crystal structure. Fig. S2 (*A–C*) represents overlays of the (*Pl*)EctA:CoA structure with that of the Ard1 acetyltransferase from the archaeon *Sulfolobus sulfataricus* P2 (PDB code 2X7B), an acetyltransferase from the bacterium *Agrobacterium tumefaciens* (PDB code 2GE3), and the human acetyltransferase NAA50 (PDB code 4X5K). This comparison highlights that the CoA-binding site in the (*Pl*)EctA:CoA crystal structure corresponds closely with the architecture(s) of typical CoA-binding sites (75, 84).

The (Pl)EctA homodimer forms the binding sites for the DAB substrate

To further understand the catalytic mechanism of (*Pl*)EctA, we determined its crystal structure bound to its substrate DAB. This structure has a resolution of 1.5 Å (Table 1) and was solved by molecular replacement using the apo-(*Pl*)EctA structure as a search model. Our structural analysis shows that the DAB substrate is located in a narrow grove that is buried inside the enzyme (Fig. 4*A*). Contrary to the CoA-binding site, parts of both monomers of (*Pl*)EctA build up the DAB-binding site. From monomer A, the loop connecting α1-α2, β4, the C terminus of β5, and the C-terminal part of the loop to β7 (Fig. 3) contributes to the binding pocket. In addition, helix α2 (particularly residue Tyr^{38}) from monomer B completes the mainly negatively charged substrate-binding pocket (Fig. 4*B* and Fig. 6*A*). DAB interacts via both oxygen atoms of the carboxyl group with the side chain of Gln^{80} and Trp^{79} (at distances of 3.0 and 3.2 Å) and the side- and main-chain atoms of Asp^{33} (at distances of 3.2 and 2.8 Å). The side chain of Asp^{33} in turn is coordinated via the side chain of His^{155} (at a distance of 2.8 Å). The DAB nitrogen is hydrogen-bonded by Asp^{33} and Glu^{158} (at distances of 3.2 and 2.7 Å), whereas the distal nitrogen atom interacts with the backbone of Trp^{79} (at a distance of 2.9 Å) (Fig. 6*A*).

To consolidate our structural assessments of the DAB-binding site, we probed the importance of seven DAB-contacting residues for (*Pl*)EctA enzyme activity via site-directed mutagenesis. We replaced each of these DAB-contacting residues separately with an Ala residue (Table 2). In an alignment of 432 *bona fide* EctA proteins (41), these seven residues are either strictly conserved or conservatively replaced by amino acid residues with similar properties. This is documented in an abbreviated alignment of 15 EctA-type proteins when (*Pl*)EctA was used as the search query (Fig. S3). For all constructed (*Pl*)EctA variants, we observed no differences in the their purification compared with the WT protein. All mutants exhibited a significantly reduced enzyme activity. Whereas the H155A, D33A, and W79A (*Pl*)EctA variants showed strongly reduced enzyme activity (remaining activities were 29.8, 8.7, and 9.9%, respectively), the other four (*Pl*)EctA variants exhibited only residual enzyme activity (<2%) (Table 2). Because Tyr^{38} of monomer B protrudes into the DAB-binding site of monomer A (and vice versa) (Fig. 4*B*) and is apparently crucial for (*Pl*)EctA enzyme activity (Table 2), we asked whether the Y38A substitution would fundamentally disturb the dimer assembly of (*Pl*)EctA. We therefore carried out a SEC-MALS analysis of the (*Pl*)EctA-Y38A variant and found that it still forms a stable dimer in solution (Fig. S4). Collectively, our mutant studies support the position and salient characteristics of the DAB-binding site that we have captured in the (*Pl*)EctA:DAB crystal complex (Fig. 6*A*).

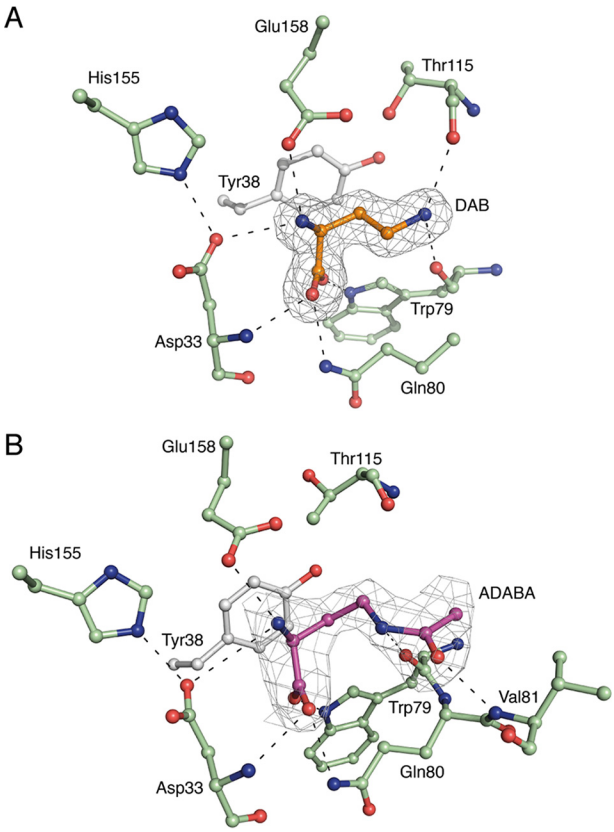

Figure 6. Architecture of the DAB substrate-binding site and coordination of the enzyme reaction product *N*-γ-ADABA. *A*, hydrogen bonds are formed between the substrate DAB and residues Asp^{33}, Tyr^{38} (monomer B), Trp^{79}, Gln^{80}, His^{155}, and Glu^{158} of the (*Pl*)EctA protein. This figure was rendered using the (*Pl*)EctA:DAB structure (PDB code 6SL8) as the template. *B*, hydrogen bonds are formed between the reaction product *N*-γ-ADABA and amino acid residues Asp^{33}, Tyr^{38} (monomer B), Trp^{79}, Gln^{80}, and His^{155}. This figure was rendered using the (*Pl*)EctA:*N*-γ-ADABA structure (PDB code 6SJY) as the template.

Table 2
Enzyme activities of the EctA variants relative to the activity of the WT (*Pl*)EctA enzyme

EctA variant	Relative enzyme activity
	%
EctA WT[a]	100
D33A	8.7 ± 3.0
Y38A	0.8 ± 1.0
W29A	9.9 ± 1.5
Q80A	0.8 ± 1.3
T115A	1.6 ± 1.9
H155A	29.8 ± 6.4
E158A	0 ± 0

[a] The enzyme activity of the (*Pl*)EctA WT enzyme was 29.08 ± 4.08 units mg^{-1} and was set for comparative reasons to 100%. Enzyme assays were conducted for the WT (*Pl*)EctA and each of its mutant derivatives with two independently prepared protein batches and in each case with two technical replicates.

Among the top hits from the DALI search with the (*Pl*)EctA crystal structure as the query, only the crystal structure of the L-2,4-diaminobutyrate acetyltransferase (EctA) from *B. parapertussis* (PDB code 3D3S) contains DAB. The (*Pl*)EctA and (*Bp*)EctA crystal structures possessed an r.m.s.d. of 1.3 Å over 156 Cα atoms when the structures were overlaid with each other (Fig. S5). However, in the (*Bp*)EctA crystal structure, the DAB-binding site is located at the interface of the two monomers (Fig. S5), whereas it is deeply buried in the two monomers of the (*Pl*)EctA crystal structure that we present here (Fig. 4*A*). DAB needs to react with acetyl-CoA for the EctA-mediated transfer of the acetyl group to form the reaction products *N*-γ-ADABA and CoA (Fig. 1*A*). Hence, one would expect the two substrates to be positioned in close proximity in the active site. In the crystal structures of the (*Pl*)EctA protein, this is indeed the case (Fig. 4*A*) (see below). However, in the (*Bp*)EctA:DAB crystal structure, the predicted position of the CoA molecule would be located at a large distance from the DAB molecule. Because the crystallization condition and a detailed description of the (*Bp*)EctA crystal structure have not yet been published, we cannot distinguish whether this is due to crystallization procedures or whether this protein contains an active site whose architecture is substantially different from that of (*Pl*)EctA. This latter possibility seems unlikely to us because the amino acid sequences of *bona fide* EctA-type proteins are highly conserved (41) (note: the (*Pl*)EctA and (*Bp*)EctA proteins possess an amino acid sequence identity of 36.4% and amino acid sequence similarity of 49.7%).

The (Pl)EctA crystal structure in complex with CoA and DAB

We succeeded in crystallizing (*Pl*)EctA in complex with both the CoA cofactor and the DAB substrate at a resolution of 1.2 Å (Table 1). Whereas (*Pl*)EctA:CoA contains only one monomer in the ASU, the ternary complex ((*Pl*)EctA:CoA:DAB) crystallized as a dimer in the ASU. This is the functional dimer, which was observed in all crystal structures when we inspected the symmetry-related molecules. In the (*Pl*)EctA:CoA and (*Pl*)EctA:CoA:DAB crystal structures, the overall fold of the protein and the binding of CoA were very similar, as evidenced by the low r.m.s.d. of 0.41 Å over 131 Cα atoms between both crystal structures. The largest difference was observed for the tail of the CoA molecule and the loop between helix α1 and α2. The β-alanine-cysteamine tail of CoA is oriented slightly outward, thereby introducing an additional hydrogen bond that is formed by the oxygen of the Ser^{31} side chain with the N4P atom in monomer A (at a distance of 2.7 Å) (Fig. 7). Through this stable interaction, the loop between helices α1 and α2 is shifted toward the CoA cofactor. In chain B of the (*Pl*)EctA:CoA:DAB structure, the CoA tail is bent more outward, such that the interactions with Asn^{120} and Ser^{31} are weakened by an increased distance to 3.7 Å. In the (*Pl*)EctA:CoA:DAB structure, the DAB substrate is located at the same position as found in the (*Pl*)EctA:DAB structure. Actually, the DAB molecule is bound by via the same set of interactions in both crystal structures (Fig. 6*A*). Hence, the (*Pl*)EctA:CoA:DAB crystal structure probably represents the transition state of the (*Pl*)EctA enzyme.

The N-γ-ADABA– binding site of the (Pl)EctA enzyme

One of the crystal structures that we obtained (PDB code 6SJY) contained the reaction product of the EctA enzyme *N*-γ-ADABA (Fig. 1*A*). This crystal structure had a resolution of 2.2 Å (Table 1). Three monomers of the (*Pl*)EctA protein are present in the ASU, and only in monomer C was the electron density in the substrate-binding pocket sufficiently defined to evaluate the correct orientation of the *N*-γ-ADABA molecule within the active site (Fig. 6*B*). *N*-γ-ADABA forms hydrogen bonds with Asp^{33}, Glu^{158}, Gln^{80}, and Trp^{79} (at distances of 3.2, 2.7, 3.3, and 3.5 Å, respectively), whereas the carbonyl oxygen of the acetyl group transferred from acetyl-CoA onto DAB to form *N*-γ-ADABA makes a hydrogen bond to the backbone nitrogen of Val^{81} (at a distance of 3.1 Å) (Fig. 6*B*). Notably, the enzyme reaction product *N*-γ-ADABA occupies essentially the same position and orientation as the substrate DAB within the active site of (*Pl*)EctA protein (Fig. 6, compare *A* with *B*).

Structures of the apo-, secondary, and ternary complex of (Pl)EctA represent different steps of the catalytic cycle

By comparing all obtained (*Pl*)EctA crystal structures, crucial steps in the catalytic cycle of the L-2,4-diaminobutyrate acetyltransferase can be visualized (Fig. 8 and Video S1). In the apo-form of the enzyme, the binding sites for the substrate DAB and the co-substrate acetyl-CoA are present in an "open" conformation (Fig. 8*A*). In this structure, there is a surface-exposed extended tunnel in which acetyl-CoA will bind, and a deep cavity is present in which DAB will be bound (Video S1). We do not know in which sequence of events the (*Pl*)EctA protein recognizes its two substrates acetyl-CoA and DAB. However, the kinetic parameters of the (*Pl*)EctA enzyme (Fig. 2, *B* and *C*) suggest that DAB might bind prior to acetyl-CoA to the protein. In the two secondary complexes that we obtained ((*Pl*)EctA:CoA and (*Pl*)EctA:DAB), the chemical groups of the two substrates involved in the acetylation reaction point toward each other (Fig. 8, *B* and *C*). In the next crystal structure, the reaction product of EctA, *N*-γ-ADABA, is captured (Fig. 8*D* and Video 1).

In the crystal structure of the (*Pl*)EctA:DAB:CoA ternary complex (Fig. 8*E*), the CoA molecule is somewhat differently orientated from the position of the CoA molecule observed in the secondary (*Pl*)EctA:CoA complex. In particular, the SH-group of CoA points in a different direction in these two complexes (Fig. 8, compare *B* with *E*). While keeping in mind that crystal structures only provide a snapshot of the various states a protein can adopt, the superimposable positions of the substrate DAB and the reaction product *N*-γ-ADABA in the (*Pl*)EctA active site (Fig. 8, compare *C* with *D*) suggest that the protein backbone and the amino acid side chains do not move substantially during enzyme catalysis. An overlay of the (*Pl*)EctA:DAB and (*Pl*)EctA:CoA crystal structures revealed a distance of $<$3.0 Å between the sulfur atom of the CoA molecule and the reactive nitrogen in the γ-position of DAB (Fig. 8*F*). This structural comparison suggests that these two secondary complexes might represent stages of the L-2,4-diaminobutyrate acetyltransferase prior to catalysis.

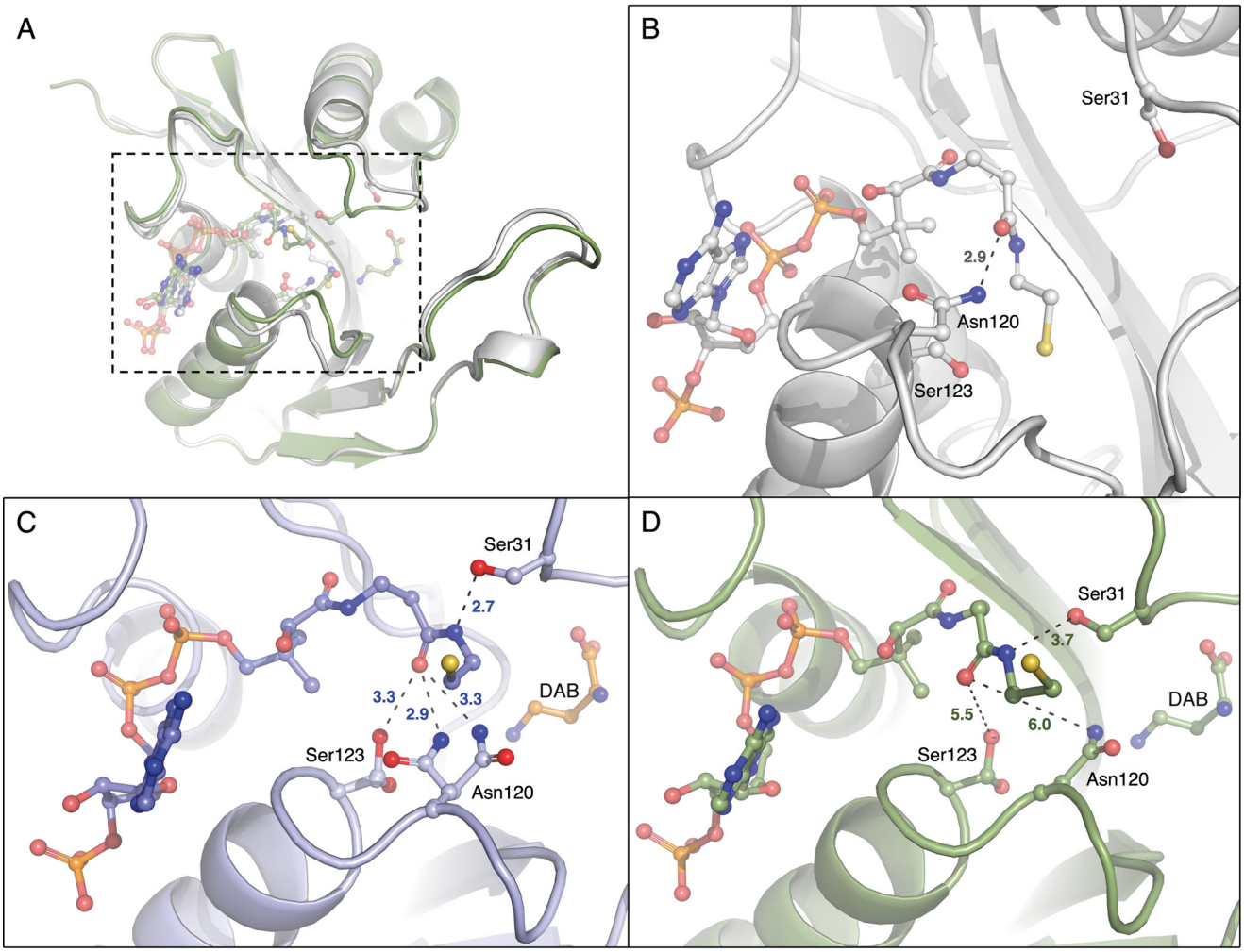

Figure 7. Conformational changes of CoA within the (*Pl*)EctA active site. *A*, overlay of (*Pl*)EctA:CoA (*gray*) (PDB code 6SK1) and (*Pl*)EctA:CoA:DAB monomer B (*green*) (PDB code 6SLL), highlighting the conformational differences in the two loops involved in CoA binding (*dashed rectangle*). The *enlarged rectangle* is shown as follows. *B*, (*Pl*)EctA:CoA (*gray*); *C*, (*Pl*)EctA:CoA:DAB monomer A (*blue*); *D*, (*Pl*)EctA:CoA:DAB monomer B (*green*). Illustrated are the slightly different conformations of CoA in the case of being the only ligand (*B*) in the (*Pl*)EctA enzyme (*gray*), and in the case of being co-crystallized along with the substrate DAB (monomer A (*blue*) in *C*; monomer B (*green*) in *D*). Asn^{120} and Ser^{123} display two alternative side-chain conformations in the (*Pl*)EctA:CoA:DAB crystal structure.

Because acetyl-CoA is highly reactive, we were not able to obtain crystal structures of the (*Pl*)EctA:acetyl-CoA, (*Pl*)EctA:acetyl-CoA:DAB, or (*Pl*)EctA:acetyl-CoA:*N*-γ-ADABA complex. Instead, in our crystal structures, the nonreactive CoA is always present (as it was added to the crystallization solutions). To visualize a possible tertiary complex in which the actual co-substrate of EctA L-2,4-diaminobutyrate acetyltransferase, acetyl-CoA, is captured ((*Pl*)EctA:acetyl-CoA:DAB), we substituted *in silico* the thiol hydrogen (-SH) of CoA with an acetyl group (-C(O)CH_3) (Fig. 8*G*). This *in silico* model visualizes how close the reactive groups of acetyl-CoA and DAB are juxtapositioned just before the transfer of the acetyl group to DAB occurs (Video S1). Release of the (*Pl*)EctA reaction products CoA and *N*-γ-ADABA from the active site would then restore the apo-form of the EctA enzyme (Fig. 8*A*).

Conclusions

The five crystal structures of the (*Pl*)EctA that we present here allow us to trace and visualize the steps of the L-2,4-diaminobutyrate acetyltransferase before and after enzyme catalysis (Fig. 8 and Video S1). Both monomers of the (*Pl*)EctA dimer are crucial for jointly building the complete architecture of the two active sites of the dimeric enzyme (Fig. 4*B*). *Bona fide* L-2,4-diaminobutyrate acetyltransferases are closely related proteins, as evidenced by the considerable degree of amino acid sequence identity (Fig. S3). Using the (*Pl*)EctA protein as the search query, it ranges between 94% for *Paenibacillus glutanolyticus* DSM5162 and 25% for *Oceanobacillus iheyensis* HTE831 among 432 inspected EctA proteins retrieved from a data set of a recent comprehensive phylogenomic analysis of *ectABC* gene clusters (41). Despite the fact that these 432 EctA proteins originate from 10 major bacterial and two archaeal phyla (41), the amino acid residues involved in the binding of the substrate DAB and the reaction product *N*-γ-ADABA are highly conserved (Fig. S3). Furthermore, the architecture of the acetyl-CoA–binding site of (*Pl*)EctA corresponds to an evolutionarily well-conserved fold found in microbial and eukaryotic acetyltransferases (75, 84). Collectively, these data suggest that the crystal structures of the EctA enzyme that we present here from *P. lautus* (77) can serve as the blueprint for a structural

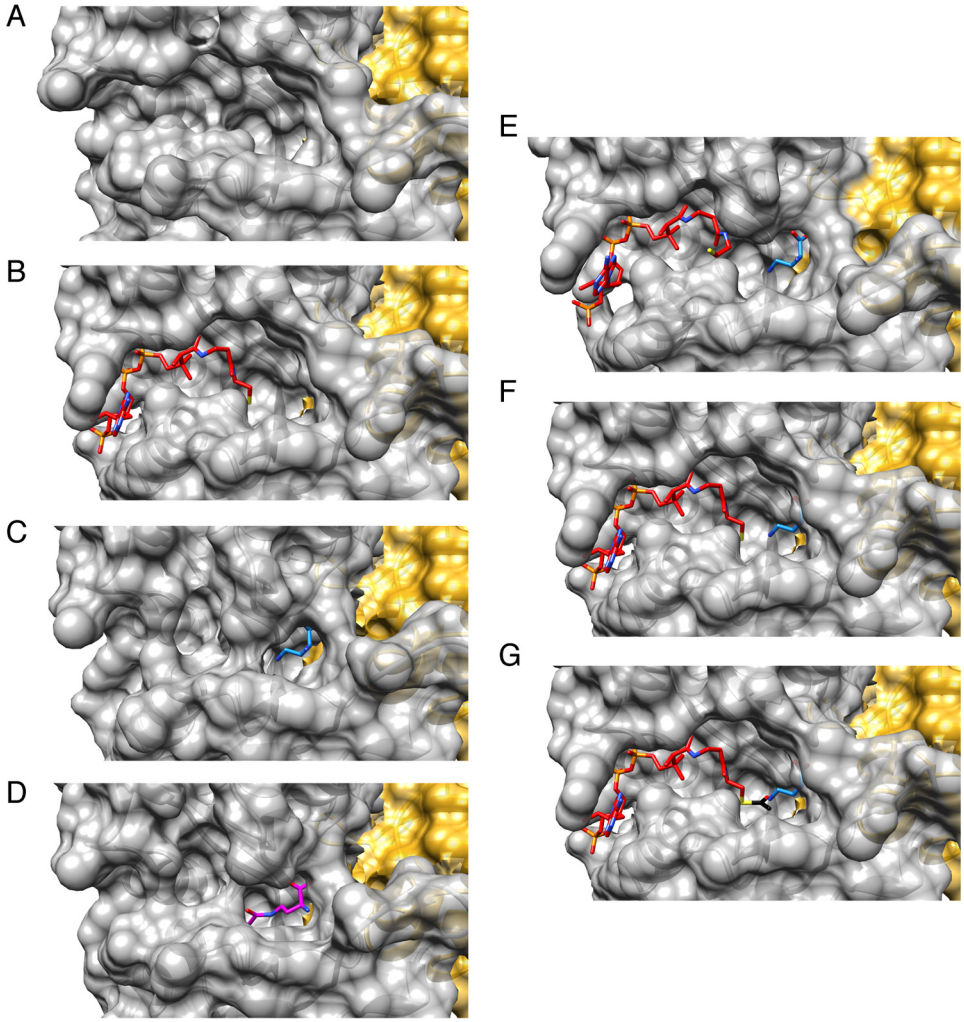

Figure 8. (*Pl*)EctA crystal structures represent different steps of the catalytic cycle. The various crystal structures of the (*Pl*)EctA protein are displayed in surface representation. *A*, apo-form of the (*Pl*)EctA enzyme with empty binding sites for DAB and acetyl-CoA. *B*, (*Pl*)EctA:CoA; only the ligand CoA (*red*) is bound in the binding tunnel. *C*, only the substrate DAB (*blue*) is bound in the active site of (*Pl*)EctA. *D*, the reaction product ADABA (*magenta*) is bound in the active site of (*Pl*)EctA. *E*, the substrate DAB (*blue*) is bound next to the ligand CoA (*red*) in the (*Pl*)EctA:CoA:DAB crystal structure, displaying a slightly different conformation of the CoA molecule found in the (*Pl*)EctA:CoA crystal structure (compare with Fig. 8). *F*, overlay of the (*Pl*)EctA:CoA crystal structure with that of the ligand DAB found in the (*Pl*)EctA:DAB crystal structure, thereby visualizing the distance (2.8 Å) between the sulfur atom from CoA and the γ-nitrogen from DAB. *G*, model of (*Pl*)EctA where an acetyl group is added *in silico* to the CoA sulfur, thereby mimicking the positions of the actual co-substrates, acetyl-CoA and DAB, in the active site of the L-2,4-diaminobutyrate acetyltransferase.

and mechanistic understanding of L-2,4-diaminobutyrate acetyltransferases in general, enzymes catalyzing the second step of ectoine biosynthesis (36, 41, 68).

From the four enzymes required for ectoine production (EctABC) and 5-hydroxyectoine (EctD) biosynthesis (26, 34, 40, 41, 45), the crystal structure of EctA now complements those of the already reported structures of ectoine synthase EctC (25) and ectoine hydroxylase EctD (71). Furthermore, an *in silico* model of EctB has also been recently established and probed by site-directed mutagenesis (69). The seminal discovery of ectoine by Galinski *et al.* (23) in the extreme halophile *Ectothiorhodospira* halochloris and of 5-hydroxyectoine by Inbar and Lapidot (24) in *Streptomyces parvulus* occurred over 30 years ago. Now, a structure-based view of the entire biosynthetic route of these remarkable stress protectants is finally at hand (Fig. 9 and Video S1). Collectively, this should aid new structure-guided attempts to improve the catalytic efficiency or stability of individual enzymes of the ectoine/5-hydroxyectoine biosynthetic route to increase industrial-scale biotechnological production of these commercially valuable chemical chaperones.

Experimental procedures

Chemicals

Ectoine was a kind gift from the bitop AG (Witten, Germany). Anhydrotetracycline hydrochloride (AHT), desthiobiotin, and Strep-Tactin Superflow chromatography material for the purification of proteins fused to a *Strep*-tag II affinity peptide were purchased from IBA GmbH (Göttingen, Germany). The reaction product of EctA, *N*-γ-ADABA, was synthesized through alkaline hydrolysis of ectoine (82). It was purified from the by-product *N*-α-ADABA by repeated chromatography on a silica gel column (Merck silica gel 60) using a gradient of ethanol/25% ammonia/water (50:1:2–10:1:2) as eluent (70). The identity and purity of *N*-γ-ADABA was monitored by TLC and NMR spectroscopy (^{1}H NMR and ^{13}C NMR) on a Bruker

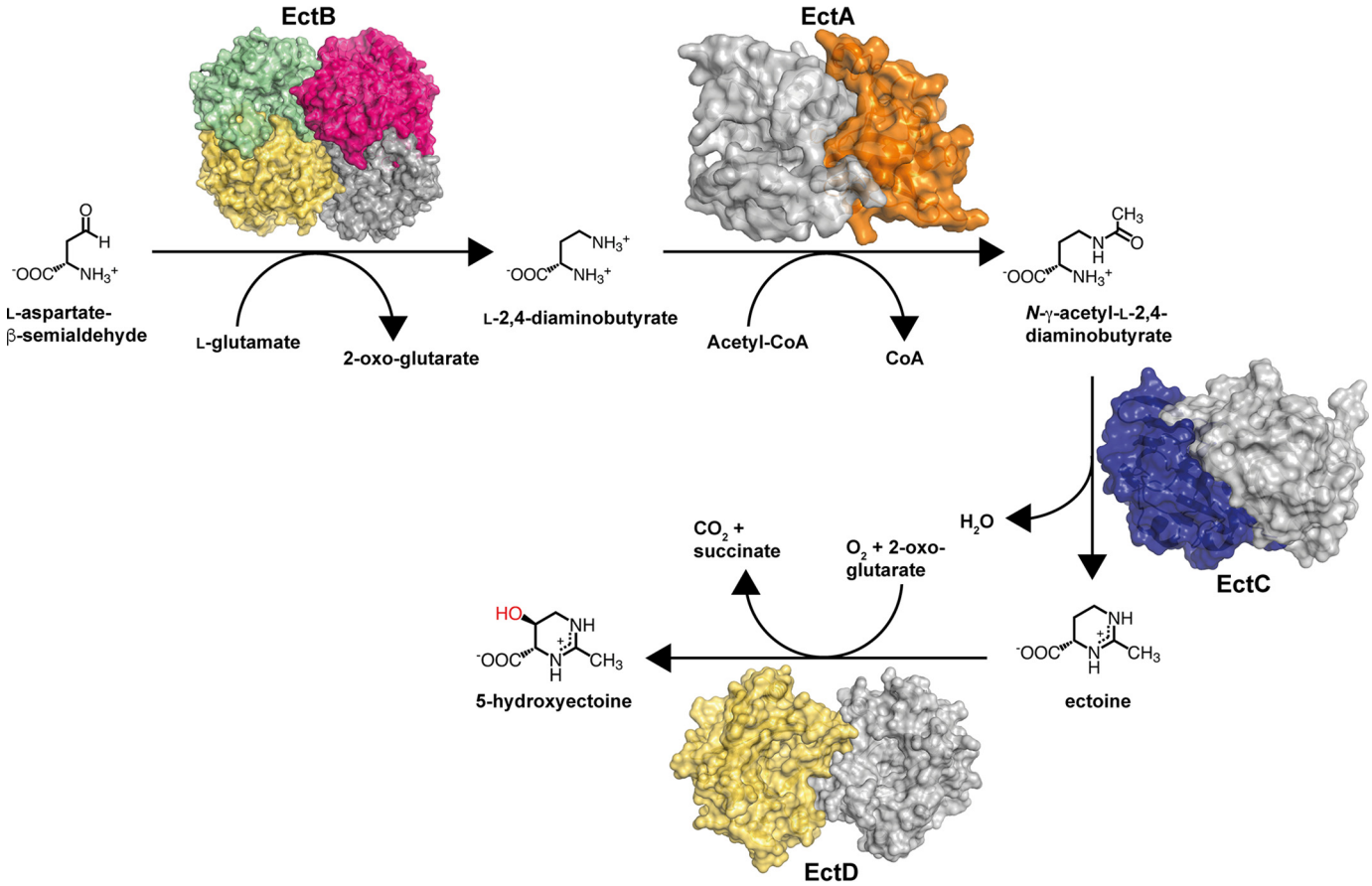

Figure 9. A structural view of the ectoine/5-hydroxyectoine biosynthetic route. The DAB aminotransferase EctB from *P. lautus* has been modeled by Richter *et al.* (69) on the crystal structure of *Arthrobacter aurescens* γ-aminobutyrate transaminase (PDB code 4ATP) (99). The crystal structure of DAB acetyltransferase EctA from *P. lautus* is reported in this publication (PDB code 6SLL). Those of the ectoine synthase EctC from *P. lautus* (PDB code 5ONM) were reported by Czech *et al.* (25), and that of the ectoine hydroxylase EctD from *Sphingopyxis alaskensis* (PDB code 4Q5O) was solved by Höppner *et al.* (71).

AVIII-400 or DRX-500 NMR spectrometer as described previously (36, 70, 82). All chemicals used to purify *N*-γ-ADABA were purchased either from Sigma–Aldrich (Steinheim, Germany) or Acros (Geel, Belgium). CoA trilithium salt was purchased from Roche Diagnostics (Mannheim, Germany). Other chemicals were obtained from Sigma–Aldrich (Taufkirchen, Germany) and Roth (Karlsruhe, Germany).

Acetyl-CoA synthesis and purification

Acetyl-CoA was synthesized from acetic anhydride (85) using a slightly modified protocol. CoA (320 mg) was dissolved in 0.5 M (8 ml) sodium bicarbonate-HCl buffer (pH 7.4). The solution was cooled down to 4 °C, and acetic anhydride (80 μl) was added dropwise under stirring. The reaction mixture was stirred for 30 min, and the completion of the reaction was confirmed by use of dithionitrobenzoic acid (DTNB) detecting the remaining free thiol groups. The reaction mixture was then acidified with formic acid until a pH of 3.0 was reached. The solution was subsequently degassed and directly applied to preparative HPLC for purification, using a preparative 1260 Infinity system (Agilent Technologies, Walsbronn, Germany). Acetyl-CoA, CoA, and other contaminants were separated using a 100 × 21-mm Gemini® 10 μM NX-C18 110-Å column (Phenomenex, Aschaffenburg, Germany) and a mobile phase system comprised of 25 mM ammonium formate (pH 4.2) and methanol. Separation was achieved using a gradient of 5–22% of methanol over 7.5 min at a flow rate of 25 ml min^{-1}. Acetyl-CoA was detected using a 1260 infinity diode array detector (at 260 nm) and a 6130 Quadrupole MS system (Agilent Technologies, Walsbronn, Germany). Fractions containing acetyl-CoA were pooled and lyophilized for 48 h. The dry powder of acetyl-CoA was freshly dissolved in water before use in enzymatic assays with the purified (*Pl*)EctA enzyme. The concentration of acetyl-CoA stock solutions was calculated from a molar extinction coefficient ($\epsilon_{260\ nm}$) for saturated acyl-CoA thioesters of 16,400 M^{-1} cm^{-1} (86).

Bacterial strains, media, and growth conditions

The *E. coli* strain TOP10 (Invitrogen) was used for the propagation of plasmids carrying *ectA* genes. Cultures of the plasmid-carrying *E. coli* strain were grown at 37 °C in Luria–Bertani liquid medium (87) containing ampicillin (100 μg ml^{-1}). Heterologous overproduction of plasmid-encoded *P. lautus* EctA proteins ((*Pl*)EctA) carrying a *Strep*-tag II affinity peptide either at the N or C terminus was carried out in the *E. coli* B strain BL21 in modified minimal medium A (87) containing 0.5% (w/v) glucose as the carbon source and 0.5% (w/v) casamino acids, 1 mM $MgSO_4$, and 3 mM thiamine as supplements.

Recombinant DNA procedures and construction of plasmids

The DNA sequence of the *ectA* gene was retrieved from the genome sequence of *P. lautus* strain Y412MC10 (accession number NC_013406.1) (77) and was used as a template for the synthesis of a codon-optimized version of the gene for its heterologous expression in *E. coli*. Synthesis of the (*Pl*)*ectA* gene was conducted by Invitrogen GeneArt (Thermo Fisher Scientific), and its DNA sequence was deposited in the GenBank™ database under accession number MF327591.1. To allow the overproduction and affinity purification of the recombinant (*Pl*)EctA protein in *E. coli*, we genetically constructed C- and N-terminal fusions of the *ectA* coding region to DNA segments encoding a *Strep*-tag II affinity peptide. For this purpose, the *ectA* gene was amplified from the plasmid (pLC46) provided by the supplier of the synthetic (*Pl*)*ectA* gene constructs using custom-synthesized primers (Table S2). The resulting PCR fragment was inserted into a pENTRY vector (IBA Göttingen, Germany), resulting in plasmid pLC48. By applying Stargate combinatorial cloning technology, the *ectA*-coding region was then inserted into the expression plasmids pASG-IBA3 and pASG-IBA5 (IBA, Göttingen, Germany), respectively; the resulting EctA overproduction plasmids were pLC50 (EctA with N-terminal *Strep*-tag II; NH_2-WSHPQFEK-SG) and pLC51 (EctA with C-terminal *Strep*-tag II; SA-WSHPQFEK-COOH). In these plasmids, expression of the recombinant (*Pl*)*ectA* gene is mediated by the *tet* promoter, whose transcriptional activity is regulated through TetR, an AHT-responsive repressor protein (IBA GmbH, Göttingen, Germany).

Site-directed mutagenesis of the (Pl)ectA gene

Mutant derivatives of the codon-optimized (*Pl*)*ectA* gene present on plasmid pLC51 were constructed by targeted mutagenesis using the Q5 Site-Directed Mutagenesis Kit (New England BioLabs GmbH, Frankfurt, Germany) with custom synthesized DNA primers purchased from Microsynth AG (Lindau, Germany). The DNA sequence of the entire coding region of each mutant (*Pl*)*ectA* gene was determined by Eurofins MWG (Ebersberg, Germany) to ensure the presence of the desired mutation and the absence of unwanted alterations. The following (*Pl*)*ectA* variants were constructed: pAR9 (GAT/GCG; D33A), pAR10 (TAT/GCG; Y38A), pAR11 (TGG/GCG; W79A), pAR12 (CAG/GCG; Q80A), pAR13 (ACC/GCG; T115A), pAR14 (CAT/GCG; H155A), and pAR15 (GAA/GCG; E158A).

Overproduction, purification, and determination of the quaternary assembly of EctA proteins

Cells of the *E. coli* B strain BL21 harboring an (*Pl*)*ectA* expression plasmid (either pLC50 or pLC51) were inoculated into modified minimal medium A containing 100 μg ml^{-1} ampicillin (1 liter of medium in a 2-liter Erlenmeyer flask) to an OD_{578} of 0.1 from an overnight preculture prepared in Luria–Bertani medium. The cells were grown on an aerial shaker (set to 180 rpm) at 37 °C until the cultures reached an OD_{578} of 0.5. At this time point, the synthetic inducer AHT of the TetR repressor was added to a final concentration of 0.2 mg ml^{-1} to trigger enhanced transcriptional activity of the *tet* promoter and thereby boost the expression of the plasmid-encoded (*Pl*)*ectA* gene. After 2 h of further growth of the culture, the *E. coli* B strain BL21 cells were harvested by centrifugation (2,360 × *g*, at 4 °C for 15 min), resuspended in 10 ml of purification buffer (100 mM Tris-HCl (pH 7.5) and 150 mM NaCl), and disrupted by passing them through a French pressure cell (16,000 p.s.i.). A cleared cell lysate of the disrupted cell was prepared by centrifugation (31,870 × *g*, at 4 °C for 45 min). The cleared cell extracts of the (*Pl*)EctA-overproducing cultures were used to purify the recombinant *Strep*-tag II–marked proteins by affinity chromatography on Strep-Tactin affinity resin as detailed previously (88, 89). The concentration of the (*Pl*)EctA protein in the individual fractions eluted from the Strep-Tactin Superflow affinity column was measured with a Nanodrop Photospectrometer ND1000 (Peqlab, Erlangen, Germany) (25,440 M^{-1} cm^{-1}). The purity and apparent molecular mass of the (*Pl*)EctA protein was assessed by SDS-PAGE (15% polyacrylamide); the PageRuler prestained protein ladder (Thermo Fisher Scientific) was used as a reference to monitor the electrophoretic mobility of the (*Pl*)EctA protein. Purified (*Pl*)EctA protein preparations were concentrated to ~10 mg ml^{-1} with Vivaspin 6 columns (Sartorius Stedim Biotech, Göttingen, Germany) with a 10-kDa molecular mass cutoff value prior to crystallization trials.

The molecular mass of (*Pl*)EctA proteins carrying a *Strep*-tag II affinity protein attached either to its N or C terminus was determined by MS analysis. 1–10 μl of a 25 mM protein solution (in purification buffer), was prepared by desalting the protein solution with a MassPrep column (Waters, Milford, MA) in a Waters ACQUITY H-Class HPLC system. Protein elution into the electrospray ionization source of a Synapt G2Si mass spectrometer (Waters) was performed at 60 °C with a flow rate of 0.1 ml min^{-1} using isocratic elution with 5% A (water/0.05% formic acid) for 2 min, followed by a linear gradient to 95% B (acetonitrile/0.045% formic acid) within 8 min and a final holding of 95% B for 4 min. The range of detected positive ions was 500–5000 *m*/*z*. For automatic drift correction, Glu-Fibrinopeptide B was measured every 45 s. Deconvolution of averaged spectra was performed after baseline subtraction and smoothing using MassLynx instrument software with MaxEnt1 extension.

To analyze the quaternary assembly of the (*Pl*)EctA protein, we used SEC-MALS. For these experiments, an Agilent Technologies system connected to a triple-angle light scattering detector (miniDAWN TREOS, Wyatt Technology Europe GmbH, Dernbach, Germany) followed by a differential refractive index detection system (Wyatt Technology) was used. Typically, 200 μl of purified (*Pl*)EctA protein (2 mg ml^{-1}) was loaded onto the Bio SEC-5 HPLC column, and the obtained data were analyzed with the ASTRA software package (Wyatt Technology).

EctA enzyme activity assays

To determine the precise reaction product of the (*Pl*)EctA enzyme (in other words whether *N*-γ-ADABA, or *N*-α-ADABA (or both) are synthesized), we carried out enzyme assays in 20 μl of 100 mM TES-HCl buffer (pH 7.5) containing 2 mM acetyl-CoA, 2 mM DAB, and 1 μg of purified enzyme at a temperature of 30 °C. The reaction was stopped after 5 min by the addition

of 20 μl of acetonitrile. The enzyme reaction product(s) were then derivatized with fluorenylmethyloxycarbonyl chloride (FMOC-Cl) using a procedure based on a previously published method (82). In brief, 2 μl of the (*Pl*)EctA enzyme reaction sample was mixed with 3 μl of an FMOC solution (25 mg ml^{-1} FMOC in acetonitrile) in a thermomixer (1 min, 900 rpm, at 20 °C). Subsequently, the FMOC reagent that had not chemically reacted was quenched by adding 6 μl of 1-aminoadamantane solution (7.6 mg ml^{-1} 1-aminoadamantane and 50% acetone in 0.5 M sodium borate buffer, pH 7.7) and mixed (1 min, 900 rpm, 20 °C). The entire solution was then diluted with 988 μl of H_2O and centrifuged (20,800 × *g*, at room temperature for 10 min) to remove the denatured (*Pl*)EctA enzyme. 37.5 μl of the supernatant was injected into an HPLC system (1260 Infinity, Agilent Technologies, Walsbronn, Germany) equipped with a 150 × 4.6-mm Gemini® 5 μM C18 110-Å column (Phenomenex, Aschaffenburg, Germany) and a fluorescence-detecting module (Agilent Technologies, Walsbronn, Germany). The fluorescence-detecting module was set to an excitation wavelength of 266 nm and an emission wavelength of 305 nm. The mobile phase consisted of solvent A (20% acetonitrile and 0.5% tetrahydrofuran in 50 mM sodium acetate buffer (pH 4.2)) and solvent B (80% acetonitrile in sodium acetate buffer (pH 4.2)). To allow the separation of the FMOC-modified *N*-γ-ADABA or *N*-α-ADABA isomers, the flow rate was set to 1 ml min^{-1} at 40 °C using a gradient of solvent A and B similar to the procedure described by Kunte *et al.* (82).

To determine the basic parameters of the (*Pl*)EctA enzyme, activity was measured at 30 °C using a continuous spectrophotometric assay. In this assay, formation of free CoA was followed using DTNB. An extinction coefficient ($\epsilon_{412\ nm}$) for DTNB of 14,000 M^{-1} cm^{-1} was used to determine the amount of CoA released during the enzyme reaction. The reaction mixture (300 μl) contained 100 mM TES-HCl buffer (pH 7.5), 1 mM DTNB, 1.2 mM acetyl-CoA, 5 mM DAB, and 0.1 μg of purified (*Pl*)EctA enzyme. The enzyme reaction was started by the addition of DAB to the reaction vessel and was run for 1.5 min, in which the absorption was determined. All (*Pl*)EctA assays were performed using two independently produced and purified protein preparations, and each protein sample was assayed twice. During the screening for the temperature profile of the (*Pl*)EctA enzyme, the reaction was started by the addition of the enzyme and was run, for high temperatures (45–60 °C), only for 0.3 min, due to reduced enzyme stability. The screening for pH optimum was performed in a 50-μl reaction volume containing a buffer mixture (MES (pH 5.5), PIPES (pH 6.5), TES (pH 7.5), CHES (pH 7.9), HEPES (pH 8.5), and CAPS (pH 10.0)) with 50 mM each, 1.2 mM acetyl-CoA, 1.7 mM DAB, and 0.1 μg of purified (*Pl*)EctA protein. The pH values of these buffer solutions and the resulting mixtures were adjusted with 37% HCl or 5 M NaOH at 30 °C. The enzyme reaction of the (*Pl*)EctA protein was started by the addition of acetyl-CoA, was run for 100 s, and was then stopped by the addition of 50 μl of 80% acetonitrile. To remove denatured (*Pl*)EctA protein, the samples were centrifuged (20,800 × *g*, at 4 °C for 5 min). For the reconstitution of a neutral pH value for the DTNB reaction, 50 μl of the supernatant was added to 150 μl of DTNB solution (0.2 M TES (pH 7.5), 2 mM DTNB), and the DTNB absorption was measured using a Tecan plate reader (Tecan Group Ltd., Männedorf, Switzerland) at 30 °C.

The kinetic parameters of the (*Pl*)EctA enzyme were determined using the continuous spectrophotometric assay described above either with 5 mM DAB and varied concentrations of acetyl-CoA (0.05–8 mM) or with 4 mM acetyl-CoA and varied concentrations of DAB (0.05–1.6 mM). The enzyme activity of the various (*Pl*)EctA mutants was monitored with the same continuous assay in a reaction containing 100 mM TES-HCl buffer (pH 7.5), 1 mM DTNB, 2 mM acetyl-CoA, 5 mM DAB, and 0.1 μg of purified (*Pl*)EctA enzyme. The enzyme activities of the (*Pl*)EctA variants were benchmarked against the WT protein whose activity was set to 100%. Under these conditions, the WT (*Pl*)EctA enzyme had an activity of 29.08 ± 4.08 units mg^{-1} protein. One unit is defined as the enzymatic conversion of 1 μM acetyl-CoA to 1 μM free CoA min^{-1} correlating with the same amount of DAB converted by the (*Pl*)EctA enzyme.

In silico analysis of EctA-type proteins

In a recent phylogenomic analysis of the distribution of *ect* biosynthetic gene clusters present in Bacteria and Archaea, a curated nonredundant data set comprising ectoine biosynthetic genes from 437 microbial species/strains was generated (41). We relied on this data set to retrieve EctA-type proteins and compared their amino acid sequences with the MAFFT multiple-amino acid sequence alignment tool (http://mafft.cbrc.jp/alignment/server/)[5] (90) using the (*Pl*)EctA protein sequence (accession number AWH98098) as the template for a BLAST search (91).

Crystallization of the (Pl)EctA protein

Several crystals were found for the apo-(*Pl*)EctA protein and the ligand-bound forms using commercial screens (Nextal, Qiagen, Hilden, Germany; Molecular Dimensions, Suffolk, UK) in 96-well sitting-drop plates (MRC3, Swissci) at 12 °C. Both the C-terminal and N-terminal *Strep*-tag II–marked forms of the (Pl)EctA protein were used in these crystallization trials. Crystals of the apo-(*Pl*)EctA protein were obtained using commercial screens and by slightly optimizing the composition of the crystallization solution. 0.1 μl of (*Pl*)EctA protein solution (10–15 mg of protein ml^{-1}) and 0.1 μl of reservoir solution were mixed and equilibrated against 40 μl of reservoir solution. For the apo-form of (*Pl*)EctA, the first crystal appeared after 12 h. The most promising condition was found with a solution containing 0.2 M lithium sulfate, 0.2 M sodium acetate, 0.1 M HEPES (pH 7.5), and 25% (w/v) PEG 4000 from the Nextal PEG II suite (Qiagen, Hilden, Germany) after 8 days. The best-diffracting crystals were grown in a solution consisting of 0.2–0.3 M lithium sulfate, 0.2 M sodium acetate, 0.1 M HEPES, pH 7.5, and 22–28% (w/v) PEG 4000. A second condition containing 0.25 M sodium sulfate, 0.1 M Bistris propane (pH 8.5), 25% PEG 3350 was also optimized by grid screening. 1 μl of (*Pl*)EctA protein solution was mixed with 1 μl of reservoir solution and equilibrated against 300 μl of reservoir solution. Crystals reached their maximum dimensions of about 100 × 200 × 50 μm^3 within 5–13 days.

Apart from the apo-form, different ligand-bound complex crystals were obtained by adding either 5 mM CoA (Sigma–

Aldrich), 20 mM DAB (Sigma–Aldrich), 20 mM *N*-γ-ADABA (25, 82), or a combination of CoA and DAB. The different substrates were preincubated with the protein for at least 30 min on ice. If two substrates were used, the first one was incubated for 5 min before the second one was added. For cryoprotection, all crystal-containing drops were overlaid with mineral oil before the crystals were harvested and flash-frozen in liquid nitrogen.

Data collection, processing, and structure determination

For the crystallographic analysis of apo-(*Pl*)EctA, crystals of the ligand-free form of (*Pl*)EctA diffracted to a maximum of 2.2 Å. The data set was collected at ID30B (ESRF, Grenoble, France) at 100 K, processed with XDS (92, 93), and phased using the automated AUTORICKSHAW pipeline (http://www.embl-hamburg.de/Auto-Rickshaw/)[5] with only the (*Pl*)EctA protein sequence as input. The resulting initial model was subsequently autobuilt using the ARPWARP webservice (https://arpwarp.embl-hamburg.de).[5] After several rounds of model building using COOT (94) and subsequent refinement using refmac5 (95) from the CCP4 suite (96), the structure of the full-length apo(*Pl*)EctA protein was modeled into the electron density.

The following procedures were used for the crystallographic analysis of the various forms of the (*Pl*)EctA protein. For the crystallographic analysis of (*Pl*)EctA:CoA: a high-resolution data set up to 1.5 Å was collected at ID29 (ESRF) at 100 K, processed with XDS, and phased via molecular replacement using the apo-(*Pl*)EctA structure as a search model. For the crystallographic analysis of (*Pl*)EctA:DAB, a high-resolution data set up to 1.5 Å was collected at ID30A-3 (ESRF) at 100 K, processed with XDS, and phased via molecular replacement using the (*Pl*)EctA:CoA structure as a search model. For the crystallographic analysis of (*Pl*)EctA:CoA:DAB, a high-resolution data set up to 1.2 Å was collected at ID29 (ESRF) at 100 K, processed with XDS, and phased via molecular replacement using the (*Pl*)EctA:CoA structure as a search model. For the crystallographic analysis of (*Pl*)EctA:*N*-γ-ADABA, a data set up to 2.2 Å was collected at ID23-1 (ESRF) at 100 K, processed with XDS, and phased via molecular replacement using the (*Pl*)EctA:CoA structure as a search model. Refinements of all complex structures were performed as described above.

Adding the substrate or the ortholog of acetyl-CoA, CoA, prior to the crystallization improved the crystal quality significantly, as reflected by the higher resolution of the obtained data sets. The (*Pl*)EctA:CoA crystal structure was solved at 1.5 Å (R_{work} and R_{free} values were 14.7 and 18.3%, respectively), the (*Pl*)EctA:DAB crystal structure at 1.5 Å (R_{work} and R_{free} values were 17.8 and 12.2%, respectively), the (*Pl*)EctA:CoA:DAB crystal structure at 1.2 Å (R_{work} and R_{free} values were 13.3 and 15.0%, respectively), and finally, the (*Pl*)EctA:ADABA crystal structure at 2.2 Å (R_{work} and R_{free} values were 16.7 and 20.1%, respectively). A summary of the data collection statistics, refinement details, and model content of these different (*Pl*)EctA crystal structures is given in Table 1. The crystal parameters, especially the unit cell dimensions and space group, differ between the crystals of apo-(*Pl*)EctA and the crystal with the substrates (Table 1), which implies that a different number of (*Pl*)EctA proteins are present in the asymmetric unit. In the asymmetric unit of apo-(*Pl*)EctA and (*Pl*)EctA:ADABA, three copies of EctA were found, whereas in (*Pl*)EctA:CoA and (*Pl*)EctA:DAB, only one monomer of the EctA protein was present, and in the crystals of (*Pl*)EctA:CoA:DAB and (*Pl*)EctA:ADABA, two EctA monomers were found.

PDB accession codes

The crystallographic data of the five (*Pl*)EctA structures reported here have been deposited in the RCSB Protein Data Bank under accession numbers 6SLK (apo-(*Pl*)EctA), 6SK1 ((*Pl*)EctA:CoA), 6SL8 ((*Pl*)EctA:DAB), 6SJY ((*Pl*)EctA:*N*-γ-ADABA), and 6SLL ((*Pl*)EctA:CoA:DAB), respectively.

Figure preparation of crystal structures

Figures of the crystal structures of the (*Pl*)EctA protein were prepared using the PyMOL software suite (97) and Chimera (98).

Author contributions—A. A. R., S. K., L. C., A. H., J. Z., L. L., J. S. D., E. B., and S. H. J. S. formal analysis; A. A. R., L. C., A. H., E. B., and S. H. J. S. visualization; A. A. R., J. Z., L. L., J. S. D., and S. H. J. S. methodology; A. A. R., L. C., A. H., J. Z., T. J. E., L. L., J. S. D., E. B., and S. H. J. S. writing-review and editing; A. H. and S. H. J. S. data curation; A. H., E. B., and S. H. J. S. writing-original draft; T. J. E., E. B., and S. H. J. S. supervision; E. B. and S. H. J. S. conceptualization; E. B. funding acquisition; E. B. and S. H. J. S. validation; E. B. and S. H. J. S. investigation; E. B. and S. H. J. S. project administration.

Acknowledgments—We cordially acknowledge the staff of beamline P13 (DESY, EMBL, Hamburg, Germany) for kind and helpful support during crystal screening, and we are equally thankful to the staff of the ID23-1, ID29, ID30B, and ID30A-3 beamlines of the European Synchrotron Radiation Facility (Grenoble, France) for expertly providing synchrotron radiation facilities. We greatly appreciate the generous gift of ectoine by the bitop AG (Witten, Germany) for our study. We thank Jochen Sohn for excellent technical assistance during EctA protein overproduction and purification. We are thankful to Dr. Uwe Linne (Department of Chemistry, Philipps-University Marburg) for performing the MS analysis of recombinant (Pl)EctA proteins; access to the MS facilities of the Department of Chemistry of the Philipps-University Marburg is gratefully acknowledged. We thank the Deutsche Forschungsgemeinschaft (DFG) for co-financing the SynaptG2Si mass spectrometer (Grant INST 160/621-1 FUGG to U. Linne and G. Bange). We appreciate the kind support of Lutz Schmitt (Institute of Biochemistry, University Düsseldorf) for this project. We are very grateful to Gert Bange for critical reading of the manuscript and many inspiring discussions. We particularly acknowledge and thank Alexander Lepak (SYNMIKRO Research Center, Philipps-University) for producing the video visualizing the predicted enzyme reaction mechanism of the L-2,4-diaminobutyrate acetyltransferase EctA.

References

1. Yancey, P. H. (2005) Organic osmolytes as compatible, metabolic and counteracting cytoprotectants in high osmolarity and other stresses. *J. Exp. Biol.* **208,** 2819–2830 CrossRef Medline
2. Burg, M. B., and Ferraris, J. D. (2008) Intracellular organic osmolytes: function and regulation. *J. Biol. Chem.* **283,** 7309–7313 CrossRef Medline
3. da Costa, M. S., Santos, H., and Galinski, E. A. (1998) An overview of the role and diversity of compatible solutes in *Bacteria* and *Archaea*. *Adv. Biochem. Eng. Biotechnol.* **61,** 117–153 CrossRef Medline

4. Bourot, S., Sire, O., Trautwetter, A., Touzé, T., Wu, L. F., Blanco, C., and Bernard, T. (2000) Glycine betaine-assisted protein folding in a *lysA* mutant of *Escherichia coli*. *J. Biol. Chem.* **275,** 1050–1056 CrossRef Medline
5. Ignatova, Z., and Gierasch, L. M. (2006) Inhibition of protein aggregation *in vitro* and *in vivo* by a natural osmoprotectant. *Proc. Natl. Acad. Sci. U.S.A.* **103,** 13357–13361 CrossRef Medline
6. Stadmiller, S. S., Gorensek-Benitez, A. H., Guseman, A. J., and Pielak, G. J. (2017) Osmotic shock induced protein destabilization in living cells and its reversal by glycine betaine. *J. Mol. Biol.* **429,** 1155–1161 CrossRef Medline
7. Street, T. O., Bolen, D. W., and Rose, G. D. (2006) A molecular mechanism for osmolyte-induced protein stability. *Proc. Natl. Acad. Sci. U.S.A.* **103,** 13997–14002 CrossRef Medline
8. Barth, S., Huhn, M., Matthey, B., Klimka, A., Galinski, E. A., and Engert, A. (2000) Compatible-solute-supported periplasmic expression of functional recombinant proteins under stress conditions. *Appl. Environ. Microbiol.* **66,** 1572–1579 CrossRef Medline
9. Lippert, K., and Galinski, E. A. (1992) Enzyme stabilization by ectoine-type compatible solutes: protection against heating, freezing and drying. *Appl. Microbial Biotechnol.* **37,** 61–65 CrossRef
10. Brown, C. R., Hong-Brown, L. Q., Biwersi, J., Verkman, A. S., and Welch, W. J. (1996) Chemical chaperones correct the mutant phenotype of the Δ F508 cystic fibrosis transmembrane conductance regulator protein. *Cell Stress Chaperones* **1,** 117–125 Medline
11. Chattopadhyay, M. K., Kern, R., Mistou, M. Y., Dandekar, A. M., Uratsu, S. L., and Richarme, G. (2004) The chemical chaperone proline relieves the thermosensitivity of a *dnaK* deletion mutant at 42 degrees C. *J. Bacteriol.* **186,** 8149–8152 CrossRef Medline
12. Diamant, S., Eliahu, N., Rosenthal, D., and Goloubinoff, P. (2001) Chemical chaperones regulate molecular chaperones i*n vitro* and in cells under combined salt and heat stresses. *J. Biol. Chem.* **276,** 39586–39591 CrossRef Medline
13. Kempf, B., and Bremer, E. (1998) Uptake and synthesis of compatible solutes as microbial stress responses to high osmolality environments. *Arch. Microbiol.* **170,** 319–330 CrossRef Medline
14. Roessler, M., and Müller, V. (2001) Osmoadaptation in bacteria and archaea: common principles and differences. *Environ. Microbiol.* **3,** 743–754 CrossRef Medline
15. Sleator, R. D., and Hill, C. (2002) Bacterial osmoadaptation: the role of osmolytes in bacterial stress and virulence. *FEMS Microbiol. Rev.* **26,** 49–71 CrossRef Medline
16. Wood, J. M., Bremer, E., Csonka, L. N., Kraemer, R., Poolman, B., van der Heide, T., and Smith, L. T. (2001) Osmosensing and osmoregulatory compatible solute accumulation by bacteria. *Comp. Biochem. Physiol. A Mol. Integr. Physiol.* **130,** 437–460 CrossRef Medline
17. Gunde-Cimerman, N., Plemenitaš, A., and Oren, A. (2018) Strategies of adaptation of microorganisms of the three domains of life to high salt concentrations. *FEMS Microbiol. Rev.* **42,** 353–375 CrossRef Medline
18. Csonka, L. N. (1989) Physiological and genetic responses of bacteria to osmotic stress. *Microbiol. Rev.* **53,** 121–147 Medline
19. Bremer, E., and Krämer, R. (2019) Responses of microorganisms to osmotic stress. *Annu. Rev. Microbiol.* **73,** 313–334 CrossRef Medline
20. Wood, J. M. (2011) Bacterial osmoregulation: a paradigm for the study of cellular homeostasis. *Annu. Rev. Microbiol.* **65,** 215–238 CrossRef Medline
21. van den Berg, J., Boersma, A. J., and Poolman, B. (2017) Microorganisms maintain crowding homeostasis. *Nat. Rev. Microbiol.* **15,** 309–318 CrossRef Medline
22. Booth, I. R. (2014) Bacterial mechanosensitive channels: progress towards an understanding of their roles in cell physiology. *Curr. Opin. Microbiol.* **18,** 16–22 CrossRef Medline
23. Galinski, E. A., Pfeiffer, H. P., and Trüper, H. G. (1985) 1,4,5,6-Tetrahydro-2-methyl-4-pyrimidinecarboxylic acid: a novel cyclic amino acid from halophilic phototrophic bacteria of the genus *Ectothiorhodospira*. *Eur. J. Biochem.* **149,** 135–139 CrossRef Medline
24. Inbar, L., and Lapidot, A. (1988) The structure and biosynthesis of new tetrahydropyrimidine derivatives in actinomycin D producer *Streptomyces parvulus*. Use of ^{13}C- and ^{15}N-labeled L-glutamate and ^{13}C and ^{15}N NMR spectroscopy. *J. Biol. Chem.* **263,** 16014–16022 Medline
25. Czech, L., Höppner, A., Kobus, S., Seubert, A., Riclea, R., Dickschat, J. S., Heider, J., Smits, S. H. J., and Bremer, E. (2019) Illuminating the catalytic core of ectoine synthase through structural and biochemical analysis. *Sci. Rep.* **9,** 364 CrossRef Medline
26. Pastor, J. M., Salvador, M., Argandoña, M., Bernal, V., Reina-Bueno, M., Csonka, L. N., Iborra, J. L., Vargas, C., Nieto, J. J., and Cánovas, M. (2010) Ectoines in cell stress protection: uses and biotechnological production. *Biotechnol. Adv.* **28,** 782–801 CrossRef Medline
27. Widderich, N., Czech, L., Elling, F. J., Könneke, M., Stöveken, N., Pittelkow, M., Riclea, R., Dickschat, J. S., Heider, J., and Bremer, E. (2016) Strangers in the archaeal world: osmostress-responsive biosynthesis of ectoine and hydroxyectoine by the marine thaumarchaeon *Nitrosopumilus maritimus*. *Environ. Microbiol.* **18,** 1227–1248 CrossRef Medline
28. Weinisch, L., Kühner, S., Roth, R., Grimm, M., Roth, T., Netz, D. J. A., Pierik, A. J., and Filker, S. (2018) Identification of osmoadaptive strategies in the halophile, heterotrophic ciliate *Schmidingerothrix salinarum*. *PLoS Biol.* **16,** e2003892 CrossRef Medline
29. Harding, T., Brown, M. W., Simpson, A. G., and Roger, A. J. (2016) Osmoadaptative strategy and its molecular signature in obligately halophilic heterotrophic protists. *Genome Biol. Evol.* **8,** 2241–2258 CrossRef Medline
30. Czech, L., and Bremer, E. (2018) With a pinch of extra salt: did predatory protists steal genes from their food? *PLoS Biol.* **16,** e2005163 CrossRef Medline
31. Fenizia, S., Thume, K., Wirgenings, M., and Phonert, G. (2020) Ectoine from bacterial and algal origin is a compatible solute in microalgae. *Mar. Drugs* **18,** E42 CrossRef Medline
32. Lo, C. C., Bonner, C. A., Xie, G., D'Souza, M., and Jensen, R. A. (2009) Cohesion group approach for evolutionary analysis of aspartokinase, an enzyme that feeds a branched network of many biochemical pathways. *Microbiol. Mol. Biol. Rev.* **73,** 594–651 CrossRef Medline
33. Stöveken, N., Pittelkow, M., Sinner, T., Jensen, R. A., Heider, J., and Bremer, E. (2011) A specialized aspartokinase enhances the biosynthesis of the osmoprotectants ectoine and hydroxyectoine in *Pseudomonas stutzeri* A1501. *J. Bacteriol.* **193,** 4456–4468 CrossRef Medline
34. Ono, H., Sawada, K., Khunajakr, N., Tao, T., Yamamoto, M., Hiramoto, M., Shinmyo, A., Takano, M., and Murooka, Y. (1999) Characterization of biosynthetic enzymes for ectoine as a compatible solute in a moderately halophilic eubacterium, *Halomonas elongata*. *J. Bacteriol.* **181,** 91–99 Medline
35. Reshetnikov, A. S., Khmelenina, V. N., and Trotsenko, Y. A. (2006) Characterization of the ectoine biosynthesis genes of haloalkalotolerant obligate methanotroph "*Methylomicrobium alcaliphilum* 20Z". *Arch. Microbiol.* **184,** 286–297 CrossRef Medline
36. Peters, P., Galinski, E. A., and Trüper, H. G. (1990) The biosyntheis of ectoine. *FEMS Microbiol. Lett.* **71,** 157–162 CrossRef
37. Bursy, J., Pierik, A. J., Pica, N., and Bremer, E. (2007) Osmotically induced synthesis of the compatible solute hydroxyectoine is mediated by an evolutionarily conserved ectoine hydroxylase. *J. Biol. Chem.* **282,** 31147–31155 CrossRef Medline
38. Prabhu, J., Schauwecker, F., Grammel, N., Keller, U., and Bernhard, M. (2004) Functional expression of the ectoine hydroxylase gene (*thpD*) from *Streptomyces chrysomallus* in *Halomonas elongata*. *Appl. Environ. Microbiol.* **70,** 3130–3132 CrossRef Medline
39. García-Estepa, R., Argandoña, M., Reina-Bueno, M., Capote, N., Iglesias-Guerra, F., Nieto, J. J., and Vargas, C. (2006) The *ectD* gene, which is involved in the synthesis of the compatible solute hydroxyectoine, is essential for thermoprotection of the halophilic bacterium *Chromohalobacter salexigens*. *J. Bacteriol* **188,** 3774–3784 CrossRef Medline
40. Kunte, H. J., Lentzen, G., and Galinski, E. (2014) Industrial production of the cell protectant ectoine: protection, mechanisms, processes, and products. *Curr. Biotechnol.* **3,** 10–25 CrossRef
41. Czech, L., Hermann, L., Stöveken, N., Richter, A. A., Höppner, A., Smits, S. H. J., Heider, J., and Bremer, E. (2018) Role of the extremolytes ectoine and hydroxyectoine as stress protectants and nutrients: genetics, phylogenomics, biochemistry, and structural analysis. *Genes* (*Basel*) **9,** 177 CrossRef Medline

42. Czech, L., Poehl, S., Hub, P., Stöveken, N., and Bremer, E. (2018) Tinkering with osmotically controlled transcription allows enhanced production and excretion of ectoine and hydroxyectoine from a microbial cell factory. *Appl. Environ. Microbiol.* **84,** e01772-17 CrossRef Medline
43. Stiller, L. M., Galinski, E. A., and Witt, E. (2018) Engineering the salt-inducible ectoine promoter region of *Halomonas elongata* for protein expression in a unique stabilizing environment. *Genes* (*Basel*) **9,** 184 CrossRef Medline
44. Calderón, M. I., Vargas, C., Rojo, F., Iglesias-Guerra, F., Csonka, L. N., Ventosa, A., and Nieto, J. J. (2004) Complex regulation of the synthesis of the compatible solute ectoine in the halophilic bacterium *Chromohalobacter salexigens* DSM 3043^{T}. *Microbiology* **150,** 3051–3063 CrossRef Medline
45. Bursy, J., Kuhlmann, A. U., Pittelkow, M., Hartmann, H., Jebbar, M., Pierik, A. J., and Bremer, E. (2008) Synthesis and uptake of the compatible solutes ectoine and 5-hydroxyectoine by *Streptomyces coelicolor* A3(2) in response to salt and heat stresses. *Appl. Environ. Microbiol.* **74,** 7286–7296 CrossRef Medline
46. Kuhlmann, A. U., Bursy, J., Gimpel, S., Hoffmann, T., and Bremer, E. (2008) Synthesis of the compatible solute ectoine in *Virgibacillus pantothenticus* is triggered by high salinity and low growth temperature. *Appl. Environ. Microbiol.* **74,** 4560–4563 CrossRef Medline
47. Salvador, M., Argandoña, M., Naranjo, E., Piubeli, F., Nieto, J. J., Csonka, L. N., and Vargas, C. (2018) Quantitative RNA-seq analysis unveils osmotic and thermal adaptation mechanisms relevant for ectoine production in *Chromohalobacter salexigens*. *Front. Microbiol.* **9,** 1845 CrossRef Medline
48. Knapp, S., Ladenstein, R., and Galinski, E. A. (1999) Extrinsic protein stabilization by the naturally occurring osmolytes β-hydroxyectoine and betaine. *Extremophiles* **3,** 191–198 CrossRef Medline
49. Kolp, S., Pietsch, M., Galinski, E. A., and Gütschow, M. (2006) Compatible solutes as protectants for zymogens against proteolysis. *Biochim. Biophys. Acta* **1764,** 1234–1242 CrossRef Medline
50. Zaccai, G., Bagyan, I., Combet, J., Cuello, G. J., Demé, B., Fichou, Y., Gallat, F. X., Galvan Josa, V. M., von Gronau, S., Haertlein, M., Martel, A., Moulin, M., Neumann, M., Weik, M., and Oesterhelt, D. (2016) Neutrons describe ectoine effects on water H-bonding and hydration around a soluble protein and a cell membrane. *Sci. Rep.* **6,** 31434 CrossRef Medline
51. Yanykin, D. V., Malferrari, M., Rapino, S., Venturoli, G., Semenov, A. Y., and Mamedov, M. D. (2019) Hydroxyectoine protects Mn-depleted photosystem II against photoinhibition acting as a source of electrons. *Photosynth. Res.* **141,** 165–179 CrossRef Medline
52. Manzanera, M., Vilchez, S., and Tunnacliffe, A. (2004) High survival and stability rates of *Escherichia coli* dried in hydroxyectoine. *FEMS Microbiol. Lett.* **233,** 347–352 CrossRef Medline
53. Tanne, C., Golovina, E. A., Hoekstra, F. A., Meffert, A., and Galinski, E. A. (2014) Glass-forming property of hydroxyectoine is the cause of its superior function as a dessication protectant. *Front. Microbiol.* **5,** 150 CrossRef Medline
54. Harishchandra, R. K., Wulff, S., Lentzen, G., Neuhaus, T., and Galla, H. J. (2010) The effect of compatible solute ectoines on the structural organization of lipid monolayer and bilayer membranes. *Biophys. Chem.* **150,** 37–46 CrossRef Medline
55. Herzog, M., Dwivedi, M., Kumar Harishchandra, R., Bilstein, A., Galla, H. J., and Winter, R. (2019) Effect of ectoine, hydroxyectoine and β-hydroxybutyrate on the temperature and pressure stability of phospholipid bilayer membranes of different complexity. *Colloids Surf. B Biointerfaces* **178,** 404–411 CrossRef Medline
56. Hahn, M. B., Meyer, S., Schröter, M. A., Kunte, H. J., Solomun, T., and Sturm, H. (2017) DNA protection by ectoine from ionizing radiation: molecular mechanisms. *Phys. Chem. Chem. Phys.* **19,** 25717–25722 CrossRef Medline
57. Schröter, M. A., Meyer, S., Hahn, M. B., Solomun, T., Sturm, H., and Kunte, H. J. (2017) Ectoine protects DNA from damage by ionizing radiation. *Sci. Rep.* **7,** 15272 CrossRef Medline
58. Meyer, S., Schröter, M. A., Hahn, M. B., Solomun, T., Sturm, H., and Kunte, H. J. (2017) Ectoine can enhance structural changes in DNA *in vitro*. *Sci. Rep.* **7,** 7170 CrossRef Medline
59. Kurz, M. (2008) Compatible solute influence on nucleic acids: many questions but few answers. *Saline Systems* **4,** 6 CrossRef Medline
60. Argandoña, M., Nieto, J. J., Iglesias-Guerra, F., Calderón, M. I., García-Estepa, R., and Vargas, C. (2010) Interplay between iron homeostasis and the osmotic stress response in the halophilic bacterium *Chromohalobacter salexigens*. *Appl. Environ. Microbiol.* **76,** 3575–3589 CrossRef Medline
61. Brands, S., Schein, P., Castro-Ochoa, K. F., and Galinski, E. A. (2019) Hydroxyl radical scavenging of the compatible solute ectoine generates two *N*-acetimides. *Arch. Biochem. Biophys.* **674,** 108097 CrossRef Medline
62. Bownik, A., and Stepnięwska, Z. (2016) Ectoine as a promising protective agent in humans and animals. *Arh. Hig. Rada Toksikol.* **67,** 260–265 CrossRef Medline
63. Bünger, J., Degwert, J., and Driller, H. (2001) The protective function of compatible solute ectoine on skin cells and its biomolecules with respect to UV-radiation, immunosuppression and membrane damage. *IFSCC Mag.* **4,** 1–6
64. Sun, H., Glasmacher, B., and Hofmann, N. (2012) Compatible solutes improve cryopreservation of human endothelial cells. *Cryo Letters* **33,** 485–493 Medline
65. Wedeking, A., Hagen-Euteneuer, N., Gurgui, M., Broere, R., Lentzen, G., Tolba, R. H., Galinski, E., and van Echten-Deckert, G. (2014) A lipid anchor improves the protective effect of ectoine in inflammation. *Curr. Med. Chem.* **21,** 2565–2572 CrossRef Medline
66. Graf, R., Anzali, S., Buenger, J., Pfluecker, F., and Driller, H. (2008) The multifunctional role of ectoine as a natural cell protectant. *Clin. Dermatol.* **26,** 326–333 CrossRef Medline
67. Schwibbert, K., Marin-Sanguino, A., Bagyan, I., Heidrich, G., Lentzen, G., Seitz, H., Rampp, M., Schuster, S. C., Klenk, H. P., Pfeiffer, F., Oesterhelt, D., and Kunte, H. J. (2011) A blueprint of ectoine metabolism from the genome of the industrial producer *Halomonas elongata* DSM 2581 T. *Environ. Microbiol.* **13,** 1973–1994 CrossRef Medline
68. Reshetnikov, A. S., Khmelenina, V. N., Mustakhimov, I. I., and Trotsenko, Y. A. (2011) Genes and enzymes of ectoine biosynthesis in halotolerant methanotrophs. *Methods Enzymol.* **495,** 15–30 CrossRef Medline
69. Richter, A. A., Mais, C.-N., Czech, L., Geyer, K., Hoeppner, A., Smits, A. H. J., Erb, T. J., Bange, G., and Bremer, E. (2019) Biosynthesis of the stress-protectant and chemical chaperone ectoine: biochemistry of the transaminase EctB. *Front. Microbiol.* **10,** 2811 CrossRef Medline
70. Widderich, N., Kobus, S., Höppner, A., Riclea, R., Seubert, A., Dickschat, J. S., Heider, J., Smits, S. H. J., and Bremer, E. (2016) Biochemistry and crystal structure of the ectoine synthase: a metal-containing member of the cupin superfamily. *PLoS ONE* **11,** e0151285 CrossRef Medline
71. Höppner, A., Widderich, N., Lenders, M., Bremer, E., and Smits, S. H. J. (2014) Crystal structure of the ectoine hydroxylase, a snapshot of the active site. *J. Biol. Chem.* **289,** 29570–29583 CrossRef Medline
72. Widderich, N., Höppner, A., Pittelkow, M., Heider, J., Smits, S. H., and Bremer, E. (2014) Biochemical properties of ectoine hydroxylases from extremophiles and their wider taxonomic distribution among microorganisms. *PLoS ONE* **9,** e93809 CrossRef Medline
73. Widderich, N., Pittelkow, M., Höppner, A., Mulnaes, D., Buckel, W., Gohlke, H., Smits, S. H., and Bremer, E. (2014) Molecular dynamics simulations and structure-guided mutagenesis provide insight into the architecture of the catalytic core of the ectoine hydroxylase. *J. Mol. Biol.* **426,** 586–600 CrossRef Medline
74. Salah Ud-Din, A. I., Tikhomirova, A., and Roujeinikova, A. (2016) Structure and functional diversity of GCN5-related *N*-acetyltransferases (GNAT). *Int. J. Mol. Sci.* **17,** E1018 CrossRef Medline
75. Vetting, M. W., S de Carvalho, L. P., Yu, M., Hegde, S. S., Magnet, S., Roderick, S. L., and Blanchard, J. S. (2005) Structure and functions of the GNAT superfamily of acetyltransferases. *Arch. Biochem. Biophys.* **433,** 212–226 CrossRef Medline
76. Reshetnikov, A. S., Khmelenina, V. N., Mustakhimov, I. I., Kalyuzhnaya, M., Lidstrom, M., and Trotsenko, Y. A. (2011) Diversity and phylogeny of the ectoine biosynthesis genes in aerobic, moderately halophilic methylotrophic bacteria. *Extremophiles* **15,** 653–663 CrossRef Medline
77. Mead, D. A., Lucas, S., Copeland, A., Lapidus, A., Cheng, J. F., Bruce, D. C., Goodwin, L. A., Pitluck, S., Chertkov, O., Zhang, X., Detter, J. C., Han, C. S., Tapia, R., Land, M., Hauser, L. J., *et al.* (2012) Complete genome sequence of *Paenibacillus* strain Y4.12MC10, a novel *Paenibacillus lautus*

strain isolated from Obsidian Hot Spring in Yellowstone National Park. *Stand. Genomic Sci.* **6,** 381–400 CrossRef Medline
78. Sahin, E., and Roberts, C. J. (2012) Size-exclusion chromatography with multi-angle light scattering for elucidating protein aggregation mechanisms. *Methods Mol. Biol.* **899,** 403–423 CrossRef Medline
79. Schulz, A., Stöveken, N., Binzen, I. M., Hoffmann, T., Heider, J., and Bremer, E. (2017) Feeding on compatible solutes: a substrate-induced pathway for uptake and catabolism of ectoines and its genetic control by EnuR. *Environ. Microbiol.* **19,** 926–946 CrossRef Medline
80. Tramonti, A., Nardella, C., di Salvo, M. L., Pascarella, S., and Contestabile, R. (2018) The MocR-like transcription factors: pyridoxal 5′-phosphate-dependent regulators of bacterial metabolism. *FEBS J.* **285,** 3925–3944 CrossRef Medline
81. Schulz, A., Hermann, L., Freibert, S.-A., Bönig, T., Hoffmann, T., Riclea, R., Dickschat, J. S., Heider, J., and Bremer, E. (2017) Transcriptional regulation of ectoine catabolism in response to multiple metabolic and environmental cues. *Environ. Microbiol.* **19,** 4599–4619 CrossRef Medline
82. Kunte, H. J., Galinski, E. A., and Trüper, H. G. (1993) A modified FMOC-method for the detection of amino acid-type osmolytes and tetrahydropyrimidines (ectoines). *J. Microbiol. Methods* **17,** 129–136 CrossRef
83. Holm, L., and Laakso, L. M. (2016) Dali server update. *Nucleic Acids Res.* **44,** W351–W355 CrossRef Medline
84. Wolf, E., Vassilev, A., Makino, Y., Sali, A., Nakatani, Y., and Burley, S. K. (1998) Crystal structure of a GCN5-related *N*-acetyltransferase: *Serratia marcescens* aminoglycoside 3-*N*-acetyltransferase. *Cell* **94,** 439–449 CrossRef Medline
85. Peter, D. M., Vögeli, B., Cortina, N. S., and Erb, T. J. (2016) A chemoenzymatic road map to the synthesis of CoA esters. *Molecules* **21,** 517 CrossRef Medline
86. Dawson, R. M. C., Elliot, D. C., Elliot, W. H., and Jones, K. M. (1986) *Data for Biochemical Research*, 3rd Ed., Clarendon Press, Oxford
87. Miller, J. H. (1972) *Experiments in Molecular Genetics*, Cold Spring Harbor Laboratory, Cold Spring Harbor, NY
88. Kobus, S., Widderich, N., Hoeppner, A., Bremer, E., and Smits, S. H. J. (2015) Overproduction, crystallization and X-ray diffraction data analysis of ectoine synthase from the cold-adapted marine bacterium *Sphingopyxis alaskensis*. *Acta Crystallogr. F Struct. Biol. Commun.* **71**, 1027–1032 CrossRef Medline
89. Hoeppner, A., Widderich, N., Bremer, E., and Smits, S. H. J. (2014) Overexpression, crystallization and preliminary X-ray crystallographic analysis of the ectoine hydroxylase from *Sphingopyxis alaskensis*. *Acta Crystallogr. F Struct. Biol. Commun.* **70**, 493–496 CrossRef Medline
90. Katoh, K., Rozewicki, J., and Yamada, K. D. (2019) MAFFT online service: multiple sequence alignment, interactive sequence choice and visualization. *Brief. Bioinform.* **20,** 1160–1166 CrossRef Medline
91. Altschul, S. F., Gish, W., Miller, W., Myers, E. W., and Lipman, D. J. (1990) Basic local alignment search tool. *J. Mol. Biol.* **215,** 403–410 CrossRef Medline
92. Kabsch, W. (2010) XDS. *Acta Crystallogr. D Biol. Crystallogr.* **66,** 125–132 CrossRef Medline
93. Kabsch, W. (2010) Integration, scaling, space-group assignment and post-refinement. *Acta Crystallogr. D Biol. Crystallogr.* **66,** 133–144 CrossRef Medline
94. Emsley, P., and Cowtan, K. (2004) Coot: model-building tools for molecular graphics. *Acta Crystallogr. D Biol. Crystallogr.* **60,** 2126–2132 CrossRef Medline
95. Murshudov, G. N., Skubák, P., Lebedev, A. A., Pannu, N. S., Steiner, R. A., Nicholls, R. A., Winn, M. D., Long, F., and Vagin, A. A. (2011) REFMAC5 for the refinement of macromolecular crystal structures. *Acta Crystallogr. D Biol. Crystallogr.* **67,** 355–367 CrossRef Medline
96. Collaborative Computational Project, Number 4 (1994) The CCP4 suite: programs for protein crystallography. *Acta Crystallogr. D Biol. Crystallogr.* **50,** 760–763 CrossRef Medline
97. DeLano, W. L. (2012) *The PyMOL Molecular Graphics System*, version 1.5.0.1, Schroedinger, LLC, New York
98. Pettersen, E. F., Goddard, T. D., Huang, C. C., Couch, G. S., Greenblatt, D. M., Meng, E. C., and Ferrin, T. E. (2004) UCSF Chimera: a visualization system for exploratory research and analysis. *J. Comput. Chem.* **25,** 1605–1612 CrossRef Medline
99. Bruce, H., Nguyen Tuan, A., Mangas Sánchez, J., Leese, C., Hopwood, J., Hyde, R., Hart, S., Turkenburg, J. P., and Grogan, G. (2012) Structures of a γ-aminobutyrate (GABA) transaminase from the *s*-triazine-degrading organism *Arthrobacter aurescens* TC1 in complex with PLP and with its external aldimine PLP-GABA adduct. *Acta Crystallogr. F Struct. Biol. Cryst. Commun.* **68,** 1175–1180 CrossRef Medline

The architecture of the diaminobutyrate acetyltransferase active site provides mechanistic insight into the biosynthesis of the chemical chaperone ectoine

Alexandra A. Richter, Stefanie Kobus, Laura Czech, Astrid Hoeppner, Jan Zarzycki, Tobias J. Erb, Lukas Lauterbach, Jeroen S. Dickschat, Erhard Bremer and Sander H. J. Smits

J. Biol. Chem. 2020, 295:2822-2838.
doi: 10.1074/jbc.RA119.011277 originally published online January 22, 2020